LC-PHSM-2000-021-TESLA
February 20, 2000

Vertex detector and flavour tagging studies for the TESLA linear collider

Richard Hawkings
DESY-FLC / Universität Hamburg

Abstract

The performance of heavy flavour tagging at the proposed TESLA linear collider detector is studied. Particular emphasis is placed on the performance of different tagging algorithms with a CCD vertex detector, including the SLD ZVTOP algorithm and multivariate techniques with neural networks. The optimisation of the vertex detector layout and track pattern recognition using the vertex detector are also explored. The vertex tagging code used in the studies has been made available, and is described in an appendix.

1 Introduction

The tagging of jets containing heavy flavours (bottom, charm and to a lesser extent τ) is of crucial importance to many physics topics to be addressed at a future high energy e^+e^- linear collider such as TESLA. These include the tagging of Higgs bosons $H \to b\overline{b}$ *vs.* $Z \to q\overline{q}$, the measurement of the smaller Higgs branching ratios $H \to c\overline{c}$ and $H \to \tau^+\tau^-$, and the identification of b-jets from top decays $t \to bW$ [1].

The LEP and SLD collaborations have shown the importance and effectiveness of b-tagging made possible using silicon microvertex detectors, both in the areas of precision physics and new particle searches. This will continue to be critical at TESLA, but the much more difficult area of charm tagging will also become important. This places much more stringent demands on the performance of the vertex detector due the smaller lifetime and softer fragmentation of charm hadrons as compared with b hadrons. The possible Z-factory run of TESLA also requires excellent vertex detector performance to fully exploit the large sample of Z^0 decays for precision electroweak and CP violation physics [2].

In the TESLA detector conceptual design report [1], two options were proposed for the vertex detector: a four or five layer charged coupled device (CCD) pixel detector based on an extrapolation from the existing SLD vertex detector, and a three layer active pixel sensor (APS) detector incorporating both barrel and endcap sections. The performance of these devices was evaluated using simple track smearing Monte Carlo and associated tagging algorithms.

This note describes extensive studies of vertex detector performance using full GEANT [3] simulation. The objectives of this work are threefold:

- To evaluate the performance of the currently proposed CCD and APS vertex detector designs in the context of heavy flavour tagging. The use of more advanced neural network tagging techniques, as employed by LEP experiments, has also been studied.
- To use these performance indicators to study possible variations in the detector geometry, particular with regard to the radius of the beampipe and first detector layer, and the optimisation of the difficult forward region at high $|\cos\theta|$.
- To study pattern recognition issues, to understand the contribution the vertex detector can make to the global pattern recognition, the need for standalone pattern recognition and the influence of accelerator induced background.

Most of the simulations have been done with variations of the CCD vertex detector option, however many of the conclusions should also be valid for APS designs. The basic layouts and simulation techniques used are described in Section 2, and their performance using various tagging techniques, including an optimised neural network based algorithm, is described in Section 3. Optimisation of the CCD vertex detector layout, particularly with respect to first layer radius and forward coverage is discussed in Section 4. The possible contribution of the vertex detector to the overall tracking pattern recognition is described in Section 5. Finally, the results are summarised and conclusions drawn in Section 6. Some technical details of the associated code, which will be made available as part of a future BRAHMS release, is described in the Appendix A. A parameterisation of some of the tagging efficiencies has also been generated, and this is described in Appendix B.

2 Layouts and Simulation

The simulations described in this note have been done with the BRAHMS 1.02 detector simulation program [5], which broadly follows the detector geometry described in the CDR [1] using GEANT [3]. In these studies, only the tracking detectors have been used, as shown in Figure 1. In more detail, the tracking detectors are:

- The vertex detector, discussed in more detail below.
- The intermediate tracker (ITC), implemented as a cylinder from r = 12–30 cm, with half length $z = 110$ cm. In these studies, the ITC has been simulated as a simple gaseous drift chamber (*e.g.* a mini-TPC), providing 16 space points from r = 13–29 cm, each with r-ϕ resolution of 50 μm and z resolution of 500 μm.
- The main time projection chamber (TPC), a cylindrical detector from r = 32–170 cm with half length of $z = 280$ cm, detecting 118 space points from r =39–162 cm with an r-ϕ resolution of 160 μm and a z resolution of 1 cm.
- A forward tracker, with disk (pixels or silicon strips) at z-positions of 40, 50, 120, 140 and 160 cm. This disks provide the main tracking in the very forward region at high $|\cos\theta|$ where few or no space points are available from the TPC.

No additional silicon layers ('SIT') between the ITC and TPC have been simulated in these studies. A uniform magnetic field of $B = 3$ T along the z axis has been used, and the effects of field inhomogeneities have not been addressed.

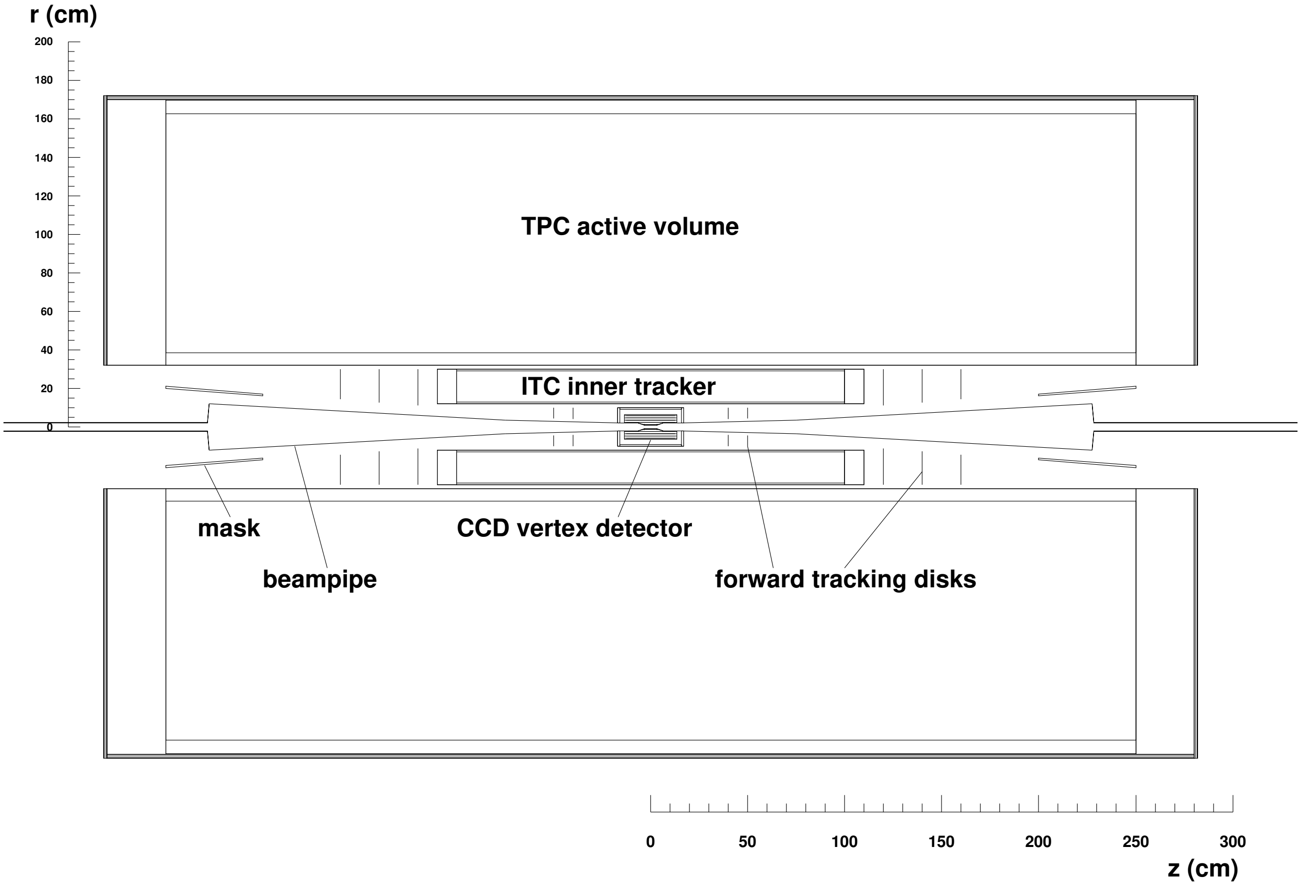

Figure 1: General layout of the tracking detectors used for this study. The CCD vertex detector option is shown.

2.1 Vertex detector layouts

Two basic vertex detector layouts have been studied, described in more detail below.

CCD vertex detector: This is a five layer pixel vertex detector using charge coupled devices, based on an extrapolation of the SLD experience. The layout is shown in Figure 2, and consists of cylindrical layers at radii of 1.2, 2.4, 3.6, 4.8 and 6.0 cm. The active parts of layers 2–5 extend to ± 12 cm in z, whilst layer 1 extends only to ± 2.5 cm in z. Each layer is 0.12 % radiation lengths thick and has readout electronics mounted on the ends beyond the edges of the z acceptance. The point resolution of each layer is $3.5\,\mu$m in both r-ϕ and r-z planes, and the whole device is mounted inside a cryostat at $r = 9$–10 cm and $z = 17$–18 cm.

The beampipe is 'necked' inwards to a radius of 1.0 cm to accommodate the innermost layer at $r = 1.2$ cm. In an alternative design, this layer is deleted, leaving 4 layers at 2.4, 3.6, 4.8 and 6.0 cm. In this case, the beampipe continues with a radius of 2.0 cm and no 'neck.' Intermediate designs, with the first layer somewhere between 1 and 2 cm, have also been studied.

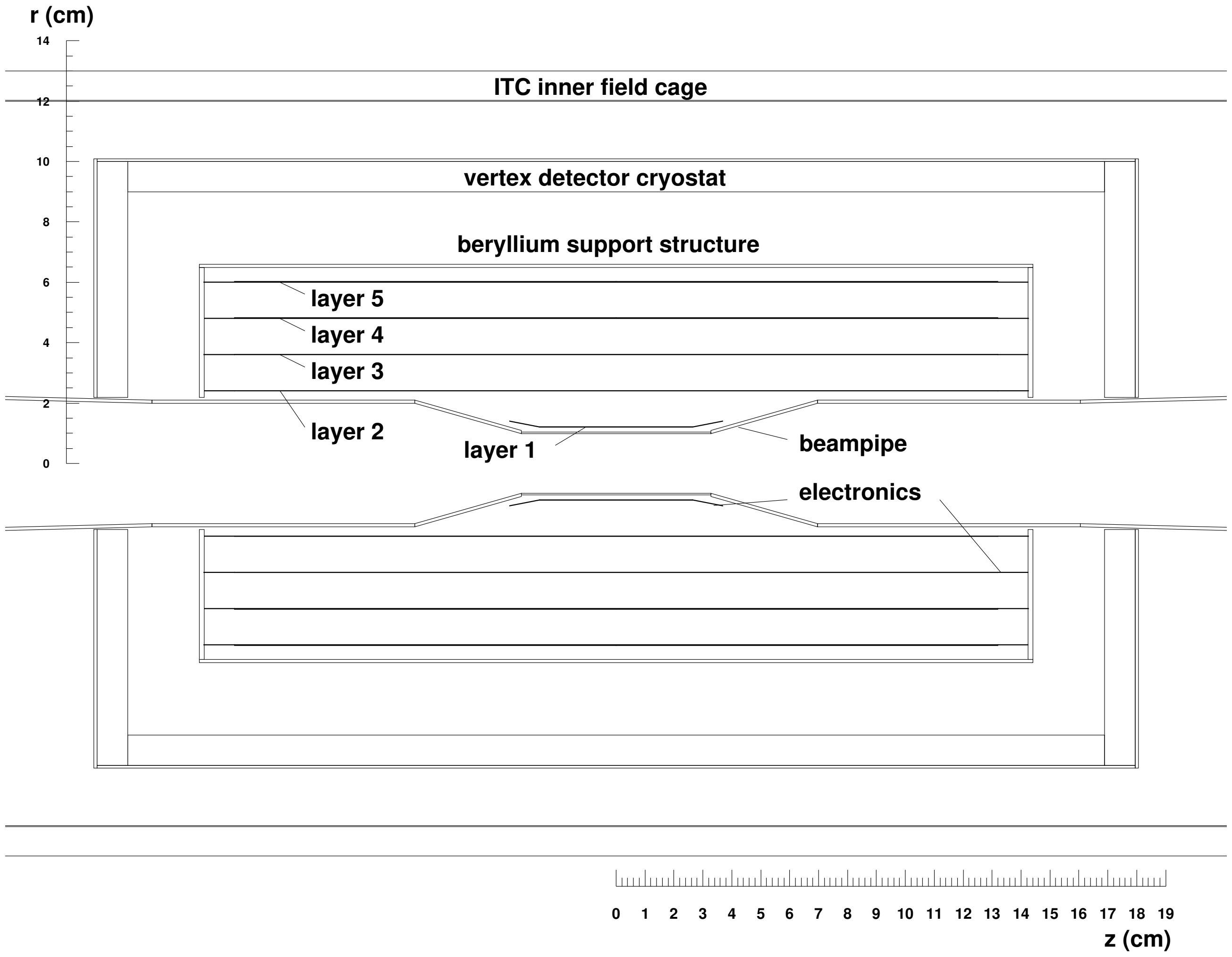

Figure 2: Layout of the 5-layer CCD vertex detector option.

APS vertex detector: This is a three layer detector, based on the technology used for the ATLAS pixel detector. Each layer has a cylindrical barrel and the outer two also have forward cones (see Figure 3). The barrels have radii of 2.5, 7.5 and 10 cm, and half lengths in z of 9.3, 13.0 and 17.3 cm. Each layer is 150 μm of silicon (0.16 % radiation lengths) and has a point resolution of 10 μm. The forward cones have the same point resolution, but a thickness of 400 μm. They have inner radii of 2.6 and 3.4 cm, outer radii of 7.5 and 10.0 cm, and half lengths of 5 cm.

2.2 Simulation and reconstruction methods

Most of the simulations have been done using $Z^0 \rightarrow q\overline{q}$ events generated at $\sqrt{s} = m_Z$ with PYTHIA 6.1 [6]. Although the linear collider will run primarily at much higher energies, the 45 GeV jets produced in Z^0 decays are typical of the energies produced in more complex

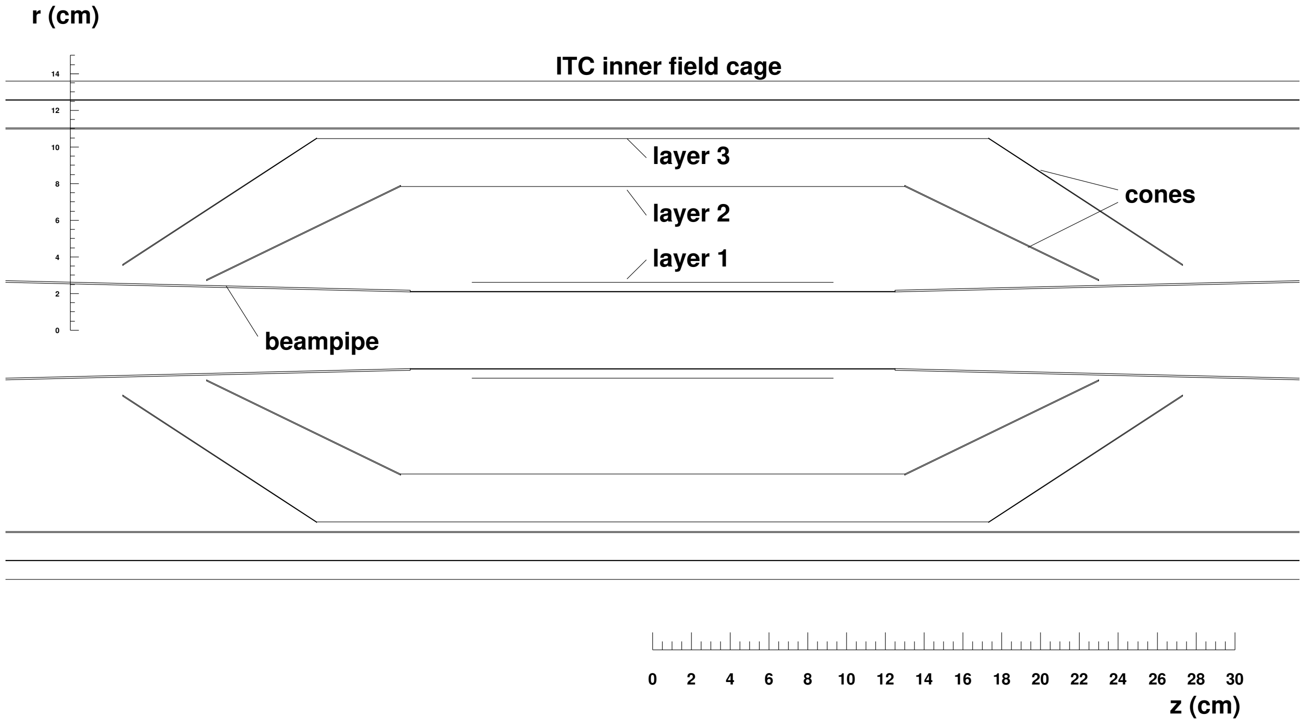

Figure 3: Layout of the 3-layer APS vertex detector option. Note that the scale of this figure is somewhat larger than that in Figure 2.

multijet final states, and provide a good benchmark for comparison with current experiments. Single particles of various momenta have also been used for some studies.

The generated events have been passed through the BRAHMS simulation of the tracking detectors, producing hits in the sensitive volumes. For most of the studies, the DELFIT track fitting package has been used to reconstruct charged tracks for subsequent analysis. This fit takes into account the effects of material interactions, but no pattern recognition is performed—an attempt is made to fit all hits which were generated by each particle. Some vertex detector pattern recognition studies are described in Section 5.

After the tracks fitting, jets were reconstructed using a cone algorithm [7] with a cone half angle of 0.65 rad and a minimum jet energy of 5 GeV. The event thrust value T and axis direction $\cos\theta_T$ were calculated using standard techniques, and events having $|\cos\theta_T| > 0.9$ were normally discarded as being outside the acceptance of the precision tracking detectors.

For many vertexing applications, an estimate of the primary vertex position is required. The primary vertex was reconstructed in each event using an algorithm based on that employed by OPAL [8]. All tracks with momentum transverse to the beamline $p_T > 0.25$ GeV and passing with 2 cm of the nominal interaction point, were fitted to a common vertex in 3 dimensions. The track with the largest χ^2 with respect to the fitted vertex was removed, and the fit repeated, until no track contributed more than four to the χ^2. With the CCD vertex detector, this algorithm reconstructs the primary vertex in $Z^0 \to q\overline{q}$ events with a resolution of 10–15 μm in x, y and z.

The primary vertex position can also be determined using a 'beamspot constraint'—*i.e.* fitting and averaging the position in many consecutive events. The precision of this method depends on the size and stability of the beamspot (collision point) itself. For the TESLA linear collider, the beamspot is expected to have dimensions of about 500 nm in x, 5 nm in y and 400 μm in z. In x and y, the effective precision of the beamspot constraint will be limited more by the detector resolution, and a 1 μm constraint has been assumed. In z, the beamspot size is much larger than the precision with which the vertex can be measured in each event, and the constraint is not useful. The resulting beamspot constraint is implemented as an extra pair of tracks (parallel to the x and y axes) in the primary vertex fit, and results in an event by event primary vertex with resolutions of 1 μm in x and y, and 10–15 μm in z.

2.3 Impact parameter resolution

One of the simplest measures of the performance of a vertex detector is the impact parameter resolution—the resolution on the distance of closest approach of a track to a particular point (*e.g.* the primary vertex or nominal interaction point). This can be defined in both r-ϕ and r-z planes (as here), or as a single quantity measured in 3 dimensions. The resolution was studied using various detector layouts—the APS detector, 4 and 5 layer CCD vertex detectors, and an intermediate 5 layer CCD detector with the beampipe at $r = 1.5$ cm and the first vertex detector layer at $r = 1.7$ cm.

Single charged pions were generated with momenta from 1–100 GeV and $|\cos\theta| < 0.9$, and processed through the simulation and track fitting. The impact parameters with respect to the nominal origin were calculated, and the resolution determined. For a set of cylindrical detectors, the r-ϕ resolution can be approximated by:

$$\sigma_{r\phi} = \sqrt{a_\phi^2 + \left(\frac{b_\phi}{p\sin^{3/2}\theta}\right)^2} \tag{1}$$

where the constant a_ϕ depends on the point resolution of the detectors, and b_ϕ represents the resolution degradation due to multiple scattering which varies with track momentum and angle. For the APS detector at high $|\cos\theta|$, this expression does not hold due to the endcap cone geometry.

The impact parameter resolution was fitted to equation 1 in bins of p and $\cos\theta$ to determine the constants a_ϕ and b_ϕ. The resulting impact parameter resolution curves are shown in Figure 4. At low track momentum p, the resolution is determined by multiple scattering, and degrades rapidly for all designs. At high momentum, the point resolution dominates, and here the two 5 layer CCD designs are very similar, irrespective of the position of the first layer. The 4 layer CCD is slightly worse, and the APS detector, with only 10 μm point resolution is much worse. Tracks in jets tend to have momenta of one or a few GeV, so the low momentum region is most important for flavour tagging. The dominance of multiple scattering means that low material and small extrapolation distances are crucial—therefore the emphasis is on placing extremely low mass detectors as close as possible to the interaction region. It should be noted that the beampipe itself is represented as a 500 μm thick beryllium cylinder, and contributes 0.14 % of a radiation length—similar to one layer of pixel detectors.

Assuming square pixel detectors, the impact parameter resolution in the r-z plane is similar to that in r-ϕ. For high momentum tracks, it is actually slightly better as there is no extrapolation error due to the track curvature. In the r-ϕ plane, where the tracks are

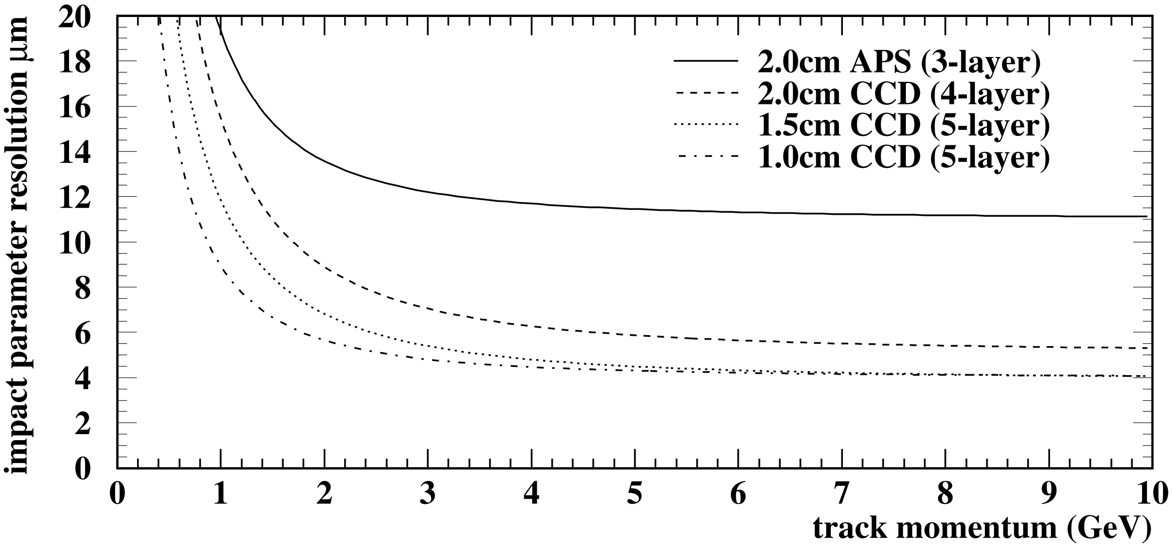

Figure 4: Track r-ϕ impact parameter resolution as a function of track momentum at $\cos\theta = 0$, for various vertex detector options (the label refers in each case to the radius of the beampipe, not the first detector layer).

bent due to the magnetic field, the curvature has to be known, and the error on the curvature measurement contributes significantly to the impact parameter resolution at high momentum.

The impact parameter resolution also varies strongly with the position of the vertex—for secondary vertices close to the first detector layer the extrapolation error is much smaller than for vertices at the origin. For 45 GeV jets, the typical b hadron decay length is 3 mm, so a significant number of b hadrons will pass through the first vertex detector layer before decaying, and this effect will increase in higher energy jets (see Section 3.7). The reconstruction of decay vertices between the vertex detector layers will therefore also be important.

3 Heavy flavour tagging

In this section, the use of the vertex detector information to tag heavy quark (bottom and charm) jets is discussed. The tagging performance is determined both by the detector performance, and by the algorithm used to distinguish b, c and light quark jets. The performance of several algorithms commonly used at LEP and SLD is evaluated, and the best results are found to be achieved using several techniques together, combined using a neural network.

3.1 Impact parameter joint probability tag

This algorithm was originally introduced by ALEPH in their R_b measurement [9]. It is a relatively simple tag, and uses the impact parameter information of each charged track in a jet (or hemisphere) to determine the probability that the track is consistent with coming from the primary vertex. The tag variable is formed by combining the probabilities of all the tracks.

In more detail, the impact parameter b of each track is signed according to whether it intersects the jet axis in front of (positive) or behind (negative) the primary vertex. Tracks from b and c hadrons, which travel a short distance before decaying, will thus tend to have positive impact parameters, whilst negative impact parameters result only from the finite detector resolution. Defining the impact parameter significance $x = b/\sigma_b$, where σ_b is the estimated error on b (calculated from the track parameter and primary vertex error matrices), the probability P_i that a track from the primary vertex has a positive impact parameter significance greater than b/σ_b is given by

$$P_i = \frac{\int_{b/\sigma_b}^{\infty} f(x)\,dx}{\int_0^{\infty} f(x)\,dx}$$

where $f(x)$ is the distribution of impact parameter significances expected for tracks with zero lifetime. In general, the symmetric function $f(x)$ can be measured from the data using tracks with negative impact parameter significance.

The joint probability P_J that an ensemble of N tracks comes from the primary vertex is then given by

$$P_J = y \sum_{m=0}^{N-1} \frac{(-\ln y)^m}{m!}$$

where y is the product of all the P_i in the ensemble. Ideally, light quark jets should then give a flat distribution of P_J between zero and one, whilst b (and to a lesser extent c) jets should give values peaked at zero.

This tagging method was implemented in the simulation and resolution functions were derived for each of the vertex detector layouts, by fitting the negative side of the impact parameter significance distributions, separately in the r-ϕ and r-z planes. The function $f(x)$ was implemented as a Gaussian plus a two component exponential tail to represent non-Gaussian effects. The results for the 5-layer CCD vertex detector are shown in Figure 5. The peaks in $P_J(r\phi)$ (P_J calculated using r-ϕ impact parameter information) and $P_J(rz)$ at zero for bottom and charm events are clearly seen. The light quark distributions are not flat due to imperfections in the resolution function tuning and correlations between the impact parameter significances of the tracks in the jet (*e.g.* due to the shared primary vertex). The spike at zero in light quark jets is caused by secondary vertices due to long lived particle decays (*e.g.* K_s and Λ). Some of these could be vetoed by an explicit search for two track vertices compatible with the K_s or Λ masses.

The impact parameter joint probabilities were used to generate the b-tagging purity *vs.* efficiency plots shown on the right in Figure 5. These and following plots have been obtained from a sample of 30 000 fully simulated $Z^0 \to q\overline{q}$ events with $|\cos\theta_T| < 0.9$. The tagging efficiency and purity are given per hemisphere, taking the jet with the most significant b-tag in each hemisphere, as in [8]. Both r-ϕ and r-z information is seen to give very good tagging performance, with high purity and efficiency. The performance obtained with the APS vertex detector is similar.

3.2 Tear down secondary vertex finder

The tagging method described above makes use of the inconsistency of the b decay tracks in coming from a single primary vertex, but does not use the information that all the b

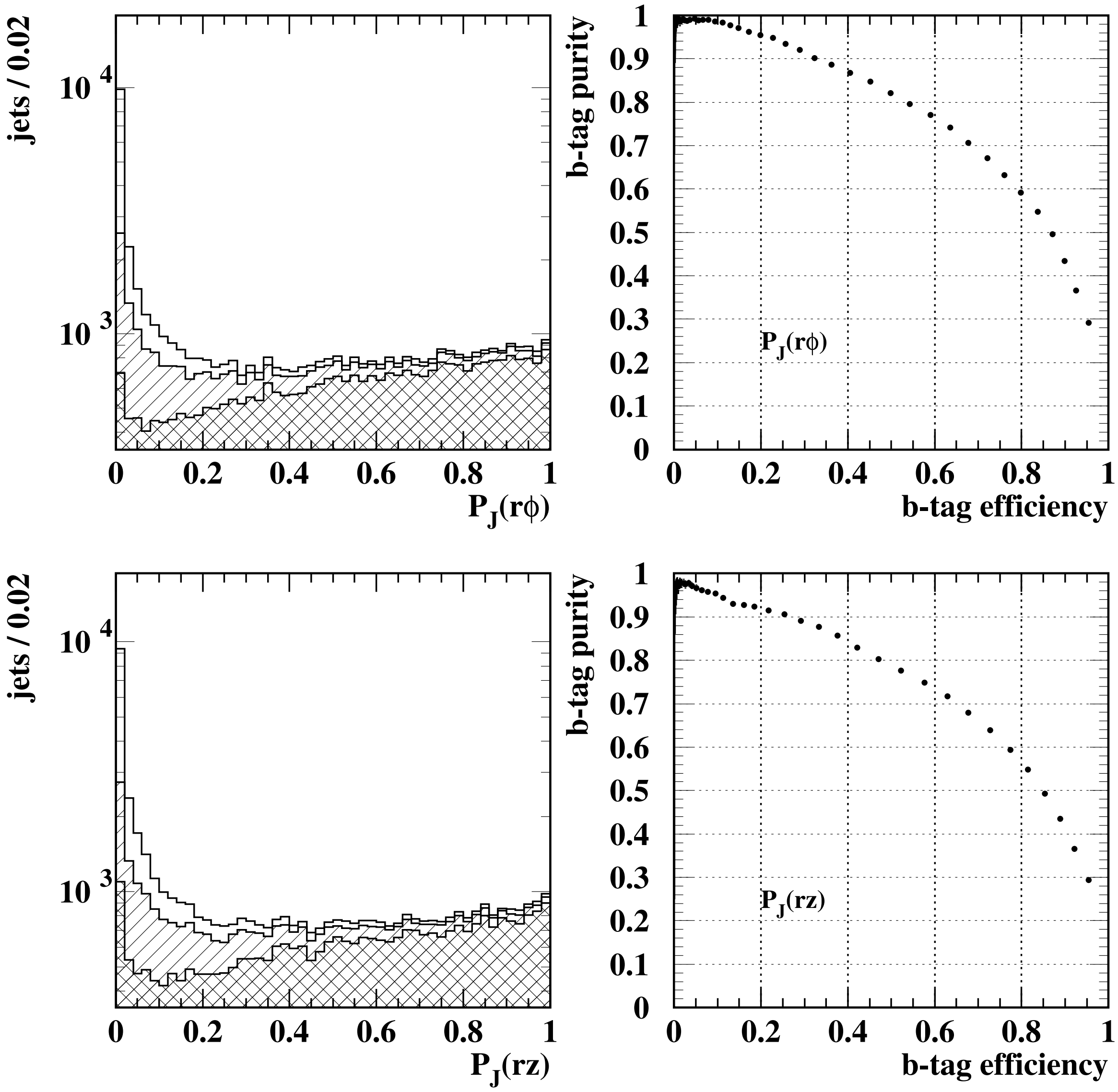

Figure 5: Performance of impact parameter joint probability tag in (top) r-ϕ plane and (bottom) r-z plane. The distributions for b, c and light quark jets are shown by the open, single and cross-hatched histograms. The b-tagging purity *vs.* efficiency curves obtained by cutting on $P_J(r\phi)$ and $P_J(rz)$ are also shown.

decay tracks should come from one or more secondary vertices. A complementary approach is offered by the b-tagging method used in OPAL [8]. Here, all well measured tracks in the jet with momentum $p > 0.5\,\mathrm{GeV}$ are fitted to a common vertex. The track contributing the largest χ^2 is removed and the fit repeated, until each remaining track contributes at most 4 to the χ^2. In OPAL, the track momentum cut combined with the high track multiplicity of b hadron decays causes the algorithm to normally converge to the b hadron decay vertex rather than the primary vertex. The distance L between the reconstructed primary and secondary vertices, and its error σ_L, are used to define the decay length significance L/σ_L, which is then used as a discriminating variable to tag b jets.

This algorithm was implemented in the simulation, with the results shown in Figure 6 for the 5 layer CCD vertex detector. By requiring at least 3 or 4 tracks to remain in the secondary vertex fit, a very pure sample of b decays is isolated at large significances. These extend up to values of several hundred, compared with up to about fifty at OPAL. However, the tagging efficiency is very disappointing, with at most only 30 % of b decays being reconstructed with a significant separated vertex. In many b decays, only a two track vertex is found, or the primary vertex is reconstructed ($L/\sigma_L \approx 0$). This results from the very high resolution vertex detectors combined with the charm hadron lifetime—many b decays do not form a single secondary vertex, but separate resolvable secondary (b) and tertiary (c) decay vertices, which are not found by the algorithm, severely limiting its efficiency. In OPAL, the tertiary vertex cannot usually be resolved, and the algorithm works much better.

3.3 Topological vertex finder ZVTOP

Neither of the above tagging methods fully exploits the performance of the vertex detector, or provides a method of tagging charm jets. The SLD collaboration, with their high resolution CCD pixel detector, has achieved excellent performance for both b and c-tagging using a different method based on topological vertex reconstruction [10]. This vertex finding code has been adapted to the linear collider software framework and the resulting performance studied.

The ZVTOP topological vertex finder is fully described in [10, 11] and only a brief description will be given here. The algorithm represents each track in the jet as a 'probability tube' in space, based on a 3-dimensional Gaussian probability density derived from the track helix parameters. A 'vertex density' is then formed from the track probability densities, and is high in regions where many tracks overlap (vertices). This vertex density is resolved into one or more separable vertices, each associated to a unique subset of tracks. One vertex is always found at the interaction point (beam spot). These vertices are then refitted using all their associated tracks, and any badly fitting tracks removed. Finally, an attempt is made to reattach unassociated tracks to the nearest vertex, allowing the reconstruction of *e.g.* 1 prong B decays where the isolated charged track gets assigned to the subsequent D decay vertex.

This procedure results in one or more reconstructed vertices, with the two vertex sample being quite pure in heavy hadron decays, and a significant number of three vertex jets, where both the secondary and tertiary vertices from the B and subsequent D hadron decay have been resolved. To distinguish bottom from charm jets, the invariant mass of the secondary (plus tertiary) vertex is calculated, and a 'p_t correction' applied [11]. The latter attempts to correct for the missing invariant mass carried away by neutral products of the B and D hadron decays, based on the difference between the vertex momentum vector calculated from the charged decay products and the vertex flight direction calculated as the direction of the

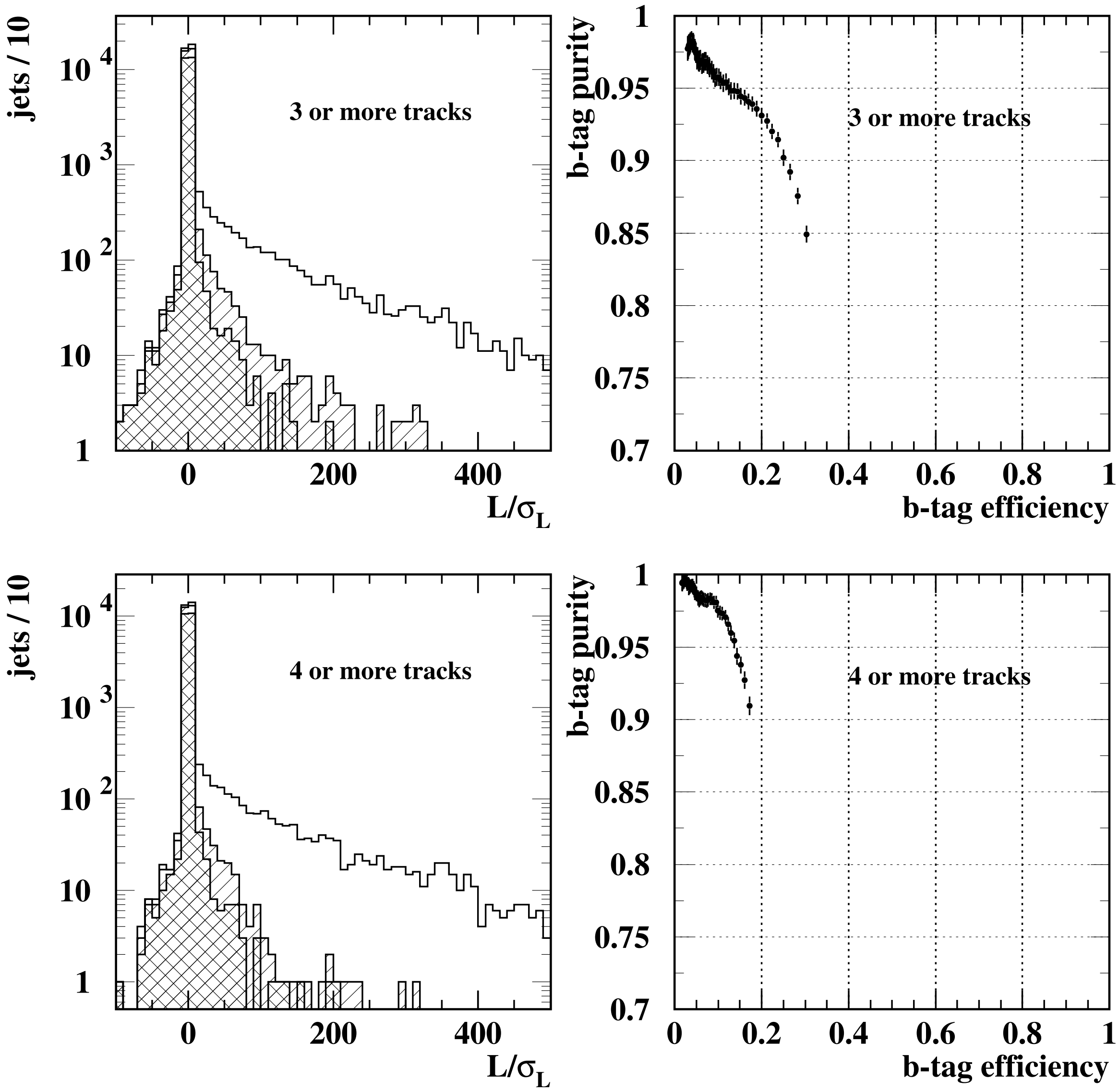

Figure 6: Performance of tear down secondary vertex finder requiring at least 3 (top) or 4 (bottom) tracks in the secondary vertex. The reconstructed decay length significance (L/σ_L) distributions are shown for b, c and light quark events as the open, single and cross-hatched histograms. The b-tagging efficiency *vs.* purity curves obtained by cutting on L/σ_L are also shown.

vector joining primary and secondary vertices.

The original SLD code was converted to standard FORTRAN and implemented into the BRAHMS framework. A small amount of performance tuning was carried out, including the removal of two track vertices compatible with the K_s mass. The parameters R_0, χ_0^2, K_{IP} and K_α were set to 0.6, 10.0, 5.0 and 1.0 as in SLD [10], and jets were accepted as heavy flavour candidates if the secondary vertex was displaced by at least $300\,\mu$m from the primary vertex. Small performance improvements may be obtained by a detailed optimisation of these values.

Some basic performance indications are given in Figure 7, for the 5 layer CCD vertex detector. The purity and efficiency of tagging b-jets by requiring that the corrected secondary vertex mass exceed a certain value is shown in Figure 7(a). By requiring that the corrected vertex mass be less than a certain value *e.g.* 2 GeV, a pure and efficient charm tag is also possible (Figure 7(b)).

The numbers of vertices reconstructed in uds, c and b events is shown in Figure 7(c), here it can be seen that most uds jets have only 1 vertex (the primary vertex), charm jets have approximately equal numbers with 1 and 2 vertices, and b jets are predominantly 2 vertex with a significant number of 3 vertex jets. The p_t corrected vertex mass distributions are shown in Figure 7(d). The high purity of high mass b jets and the sharp cut off at around 2 GeV for charm jets can clearly be seen. There is a small residual contamination of uds and charm jets at high masses, caused by miss-measured tracks and fragmentation tracks being mistakenly included in the secondary vertex. This limits the b-tag purity to around 97 %, although this should be improved with better tuned track reconstruction—SLD have achieved purities in excess of 98 % [11].

3.4 One-prong charm tag

About half the charm jets shown in Figure 7 have no reconstructed secondary vertex and so cannot be tagged using the mass tag algorithm. However, around 40 % of D^+ hadrons decay to only one charged track, so the presence of a single high momentum track with large impact parameter may be used as an additional 'one-prong' charm tag. Significant backgrounds arise from tracks with large impact parameters produced in photon conversions and K_s decays, and from mismeasured tracks.

This tagging method was applied to jets reconstructed with only one ZVTOP vertex. All tracks with momentum $p > 2$ GeV and hits in all five vertex detector layers were considered as one prong charm candidates, and sorted by their impact parameter significances in r-ϕ and r-z. Tracks identified as coming from photon conversion or K_s candidates were removed. The latter were found by forming all two track vertices from pairs of tracks with impact parameter significances $d_0/\sigma_{d_0} > 3$, and accepting vertices with a vertex probability exceeding 1 %, a radius of less than 2 cm and an invariant mass satisfying $m_{e^+e^-} < 0.02$ GeV (for photon conversions) or $0.475 < m_{\pi^+\pi^-} < 0.525$ GeV (for K_s decays).

The resulting distributions of largest and second largest track impact parameter significances in r-ϕ and r-z are shown in Figure 8. Charm events tend to have a single track with large impact parameter significance, whereas b events tend also to have a second significant track. The most important background is from from large impact parameter tracks in uds events. This information has not been used to tag charm directly, but as part of a neural network based tag discussed below.

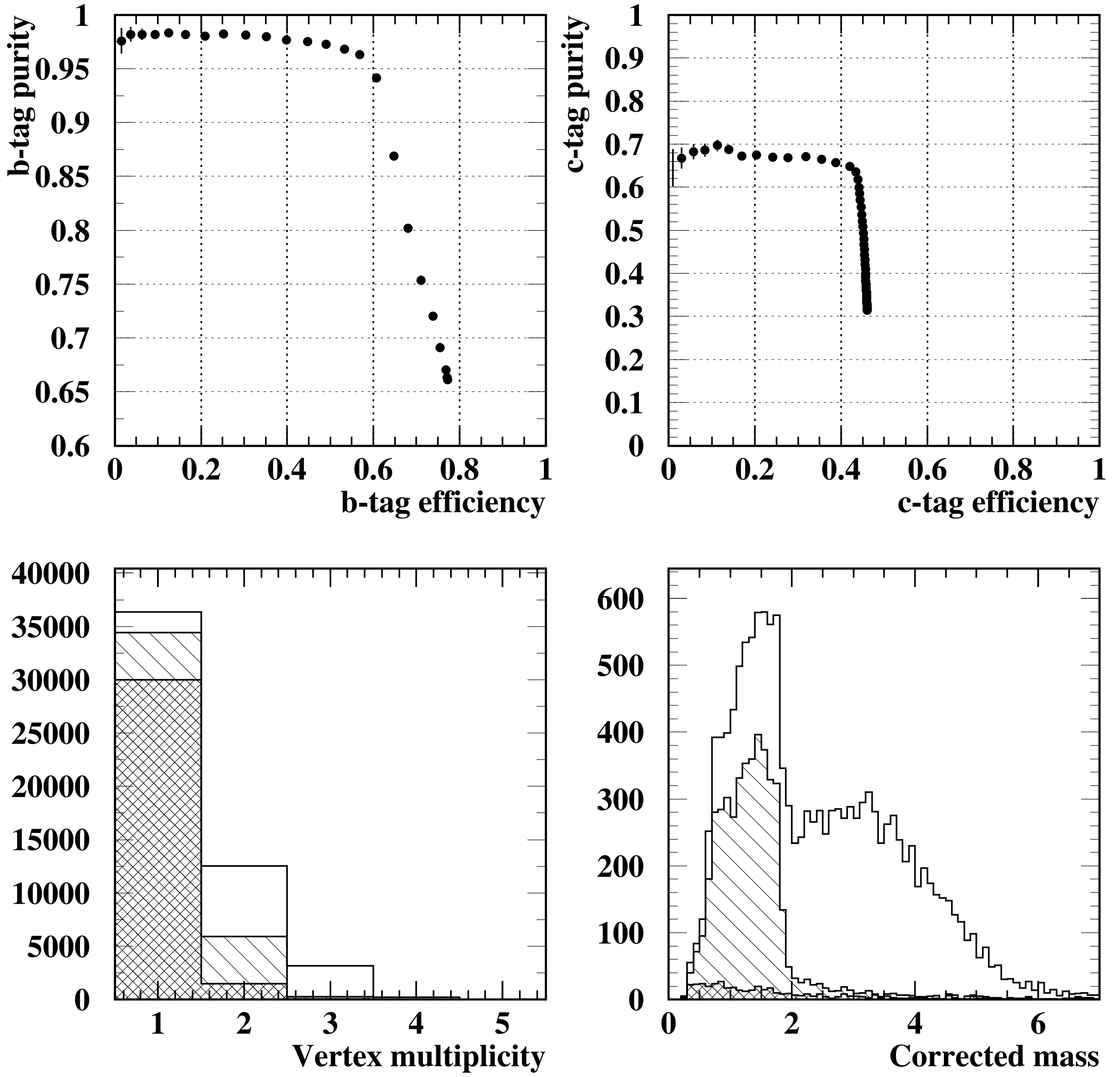

Figure 7: Performance of the ZVTOP topological vertex finding algorithm on $Z^0 \to q\overline{q}$ events, using the corrected mass to tag b and c jets. The vertex multiplicity and corrected mass distributions are also given, for b, c and light quark events, shown as open, hatched and cross-hatched histograms.

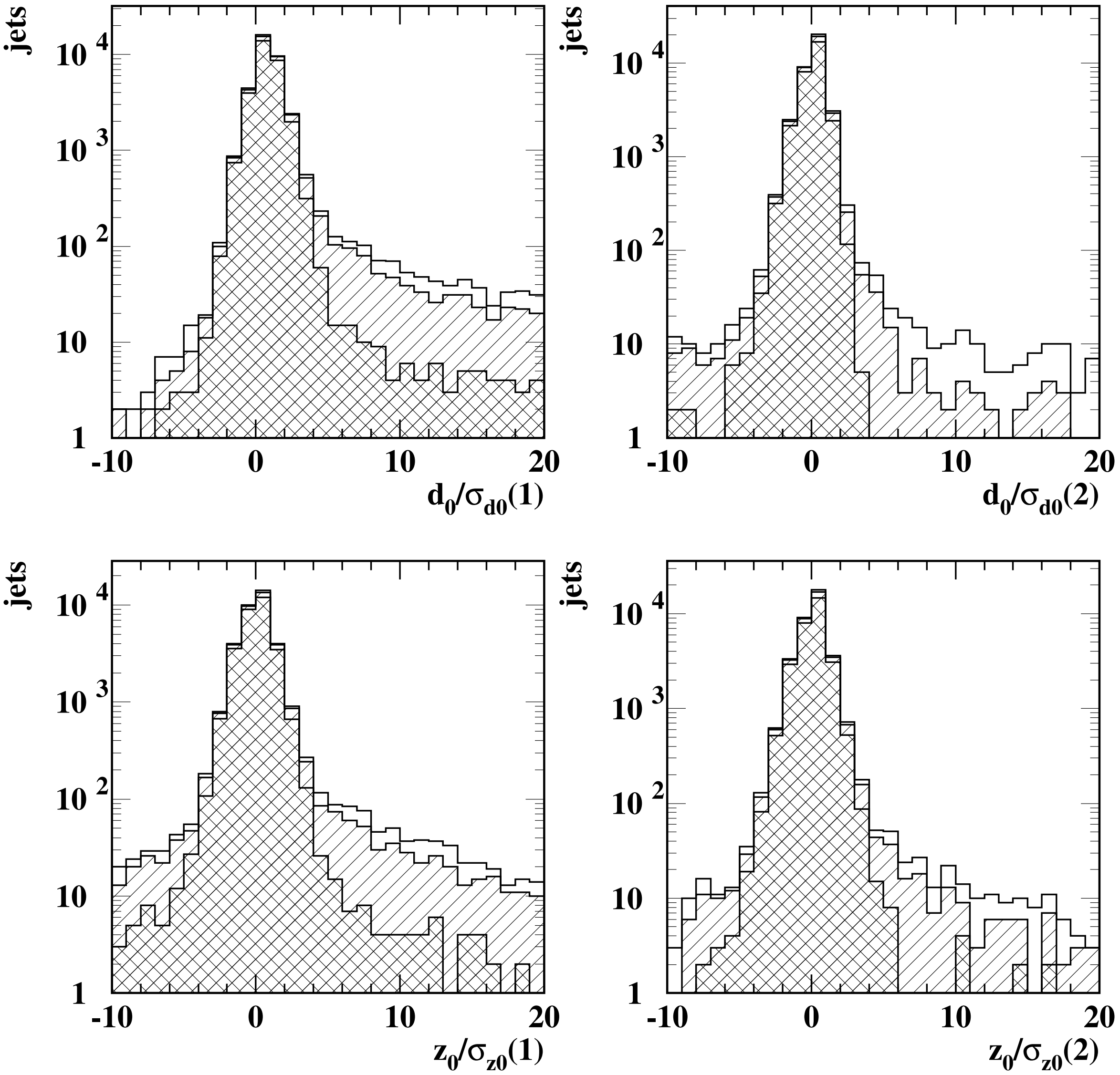

Figure 8: Distributions of most significant ($d_0/\sigma_{d_0}(1)$) and second most significant ($d_0/\sigma_{d_0}(2)$) r-ϕ impact parameters, and associated r-z impact parameters ($z_0/\sigma_{z_0}(1)$ and $z_0/\sigma_{z_0}(2)$) for jets reconstructed with only one vertex with ZVTOP. The contributions from b, c and uds jets are shown by the open, single and cross-hatched histograms.

Variable	Transformation	Charm tag figure of merit F		
		1 vertex	2 vertices	3 vertices
$P_J(r\phi)$	$P_J(r\phi)$	0.046	0.090	0.019
$P_J(rz)$	$P_J(r\phi)$	0.042	0.100	0.014
$d_0/\sigma_{d_0}(1)$	$\tanh(d_0/\sigma_{d_0}(1)/100)$	0.100	-	-
$d_0/\sigma_{d_0}(2)$	$\tanh(d_0/\sigma_{d_0}(2)/100)$	0.024	-	-
$z_0/\sigma_{z_0}(1)$	$\tanh(z_0/\sigma_{z_0}(1)/100)$	0.085	-	-
$z_0/\sigma_{z_0}(2)$	$\tanh(z_0/\sigma_{z_0}(2)/100)$	0.023	-	-
L/σ_L	$\tanh((L/\sigma_L)/300)$	-	0.095	0.042
L	$\tanh(L)$	-	0.033	0.009
m_v	$\tanh(m_v/5\,\mathrm{GeV})$	-	0.476	0.173
p_v	$\tanh(p_v/45.6\,\mathrm{GeV})$	-	0.001	0.011
n_s	$\tanh(n_s/10)$	-	0.141	0.023
P_s	P_s	-	0.068	-

Table 1: Neural network inputs and transformations used for b and c tagging. The figures of merit F for the individual inputs are given, for charm tagging in Z^0 decays.

3.5 Neural network tags

The above discussion has identified several methods of tagging b and c-jets, which can be combined to produce the most performant tags. A combination using a neural network technique has been studied here, similar to that used by OPAL [8]. Likelihood based techniques, as employed by DELPHI [12], can also be used.

The tag is based on the results of the impact parameter joint probability, ZVTOP and one prong charm tagging algorithms described above. Different tagging variables are used depending on the number of vertices identified by ZVTOP—the sample is divided into 1 vertex (primary only), 2 vertices (primary and single secondary) and 3 (or more) vertices (primary, secondary and tertiary). The various inputs used for the different cases are listed in Table 1 and described below. The networks were implemented with the JETNET 3.1 package [13] and trained using 60 000 fully simulation Z^0 decays. The transformations given in Table 1 were used on some of the variables to bring them into the ranges $-1 < x < 1$ or $0 < x < 1$ which improves the network training performance.

To evaluate the relative importance of each variable x, a 'figure of merit' F, related to the overlap of the the variable distributions for signal and background events, was used. The value of F measures the difference in signal $f_1(x)$ and background $f_2(x)$ distributions—if $F \approx 0$, the distributions are similar and the variable has no separation power, and if $F = 1$ the signal and background distributions have no overlap and complete separation is possible. F is defined by the 'inverse correlation integral'

$$F = \alpha_1 \alpha_2 \int \frac{(f_1(x) - f_2(x))^2}{\alpha_1 f_1(x) + \alpha_2 f_2(x)} \, \mathrm{d}x$$

where the signal contributes a fraction α_1 of the sample with normalised distribution $f_1(x)$, and the background contributes a fraction $\alpha_2 = 1 - \alpha_1$ of the sample with normalised distribution $f_2(x)$ [14]. The figures of merit F for each input are also given in Table 1, for the most difficult case of charm tagging in Z^0 events (*i.e.* the separation of charm jets from uds and bottom jets).

The various neural network inputs are:

Impact parameter joint probabilities $P_J(r\phi)$ and $P_J(rz)$. These are always available and used regardless of the number of vertices found by ZVTOP.

Track impact parameter significances $d_0/\sigma_{d_0}(1)$ *etc.* These variables form the one-prong charm tag, and are used together with the impact parameter joint probabilities in the case that no secondary vertices are found by ZVTOP.

Vertex decay length significance L/σ_L. The distance from the primary vertex to the furthest secondary or tertiary vertex, divided by its measurement error.

Vertex decay length L. The distance from the primary vertex to the furthest secondary or tertiary vertex—this provides a small amount of extra information in addition to L/σ_L.

Vertex mass m_v. This is the p_t corrected vertex invariant mass shown in Figure 7(d), and is by far the most powerful tagging variable for distinguishing bottom from charm jets.

Vertex momentum p_v. Although not useful on its own, this provides some additional information in conjunction with the decay length, due to the differing fragmentation functions of bottom and charm hadrons.

Secondary vertex multiplicity n_s. The total number of tracks in all secondary and tertiary vertices.

Secondary vertex probability P_s. The probability that all the tracks assigned to the secondary vertex actually come from one common vertex—derived from the χ^2 of the vertex fit. This variable provides some sensitivity to b decays with short tertiary decay lengths where the charm hadron decays close to the b decay vertex. In such cases, the secondary vertex fit probability may be reduced even though the secondary and tertiary vertices cannot be resolved separately.

Three sets of neural networks were trained using the above inputs—a b tagging network designed to separate b jets from charm and uds jets in Z^0 decays, a c tagging network designed to separate charm jets from b and uds jets in Z^0 decays, and a b/c separation network designed simply to separate b from c jets. The latter is a much simpler task, since in this case any jet not resembling a b-jet can be classified as a c-jet, whereas charm in Z^0 decays must be picked out from 'between' zero lifetime uds jets and long lifetime b-jets. The performance of the b/c separation may be more relevant than the Z^0 charm tagging when studying *e.g.* $H \to c\bar{c}$ *vs.* $H \to b\bar{b}$. The final figures of merit for the neural network output distributions are shown in Table 2 for each case. It can be seen that good separation (high values of F) can be achieved for the 2 and 3 vertex jets, but the separation in 1 vertex jets is much poorer. However, as can be seen from Figure 7(c), the latter class contains mainly light quark jets and is therefore of lesser interest.

3.6 Tagging performance

The performance of the neural network based bottom and charm tags in Z^0 decays is shown in Figure 9, and compared to the performance of the simple ZVTOP mass tags. For b-tagging, requiring at least 2 vertices to be found and cutting on the neural network output

Tag	Figure of merit F 1 vertex	2 vertices	3 vertices
b tag in Z^0 decays	0.227	0.581	0.411
c tag in Z^0 decays	0.109	0.592	0.397
b/c separation	0.168	0.627	0.393

Table 2: Figures of merit F for bottom and charm tagging neural networks for jets with 1,2 and 3 reconstructed ZVTOP vertices.

gives similar performance to the mass tag at high purity, but a 10–15 % efficiency advantage at high efficiency. Requiring at least 3 vertices to be found does not produce a significantly higher purity and severely limits the efficiency. The maximum attainable purity is somewhat limited due to the relatively small size of the neural network training sample and the influence of badly reconstructed tracks—with better training and performance tuning a somewhat higher purity should be achieved. The performance of the b-tag is not strongly affected by the choice of layout—similar results are achieved by both the 4 layer CCD and the APS detector layouts.

The performance of the mass and neural network based charm tags is also shown in Figure 9. Here, the neural network approach gives a spectacular improvement in performance over the simple mass tag—both in the high purity region, where the combination of several variables from ZVTOP is important, and at high efficiency, where the 'one-prong' tag variables help to boost the efficiency beyond the 'knee' of the pure mass tag approach.

The charm tag performance is also much more sensitive to the choice of vertex detector layout, as can be seen from Figure 10. Both the mass tag and the neural network tag benefit from the better impact parameter resolution of the 4 and 5 layer CCD detectors, which helps in both low and high efficiency regions. Therefore, the charm tag performance offers a good 'benchmark' process to evaluate various vertex detector options.

The performance of the 'b-c separation' charm tag with no uds jets is shown in Figure 11. The performance of the mass tag is rather similar to before, since few uds jets are selected in the sample with at least two reconstructed vertices. However, the neural network tag now achieves even better performance, since the one vertex jets are also used. The two Figures 10 and 11 represent two different extremes—where the background is dominated by uds jets and b jets respectively. In a real application, the optimal performance will be achieved by training the neural networks with a mixture of uds and b background appropriate to the events under study.

3.7 Energy dependence

The results described above have all been obtained from Z^0 decays, where the typical jet energy is close to 45 GeV. These energies are representative of those expected in multijet signatures at a moderate energy linear collider, *e.g.* $t\bar{t} \to 6$ jets and $ZH \to 4$ jets. However, it is clearly of interest to study the change in performance with increasing jet energy.

For this purpose, samples of 40 000 'monojet' events were generated by hadronising single quarks in JETSET, at 45, 70, 100, 200 and 300 GeV, distributed uniformly with $|\cos\theta| < 0.9$. The b and c-tagging algorithms were then applied to these jets, without adjusting any parameters or neural network tunings from those used on Z^0 events. The results are shown in Figure 12. The performance is compared by studying the efficiencies for tagging the 'wrong' flavours as a function of the efficiency for tagging the 'right flavour', rather than in terms of

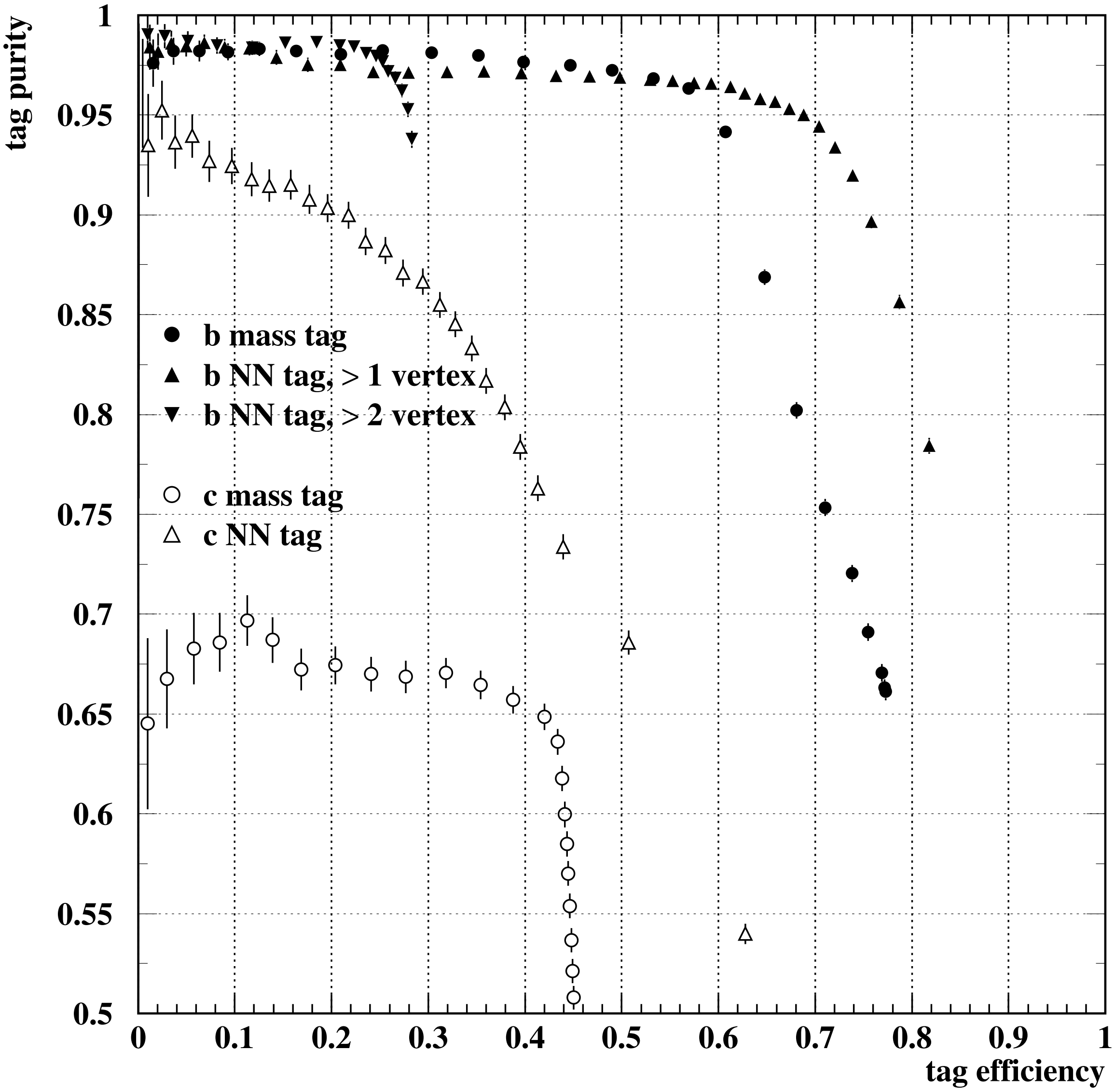

Figure 9: Efficiency *vs.* purity curves for bottom and charm tags in Z^0 decays, based on vertex mass and neural networks. The curves are for all jets with $|\cos\theta| < 0.9$ using the 5 layer CCD vertex detector.

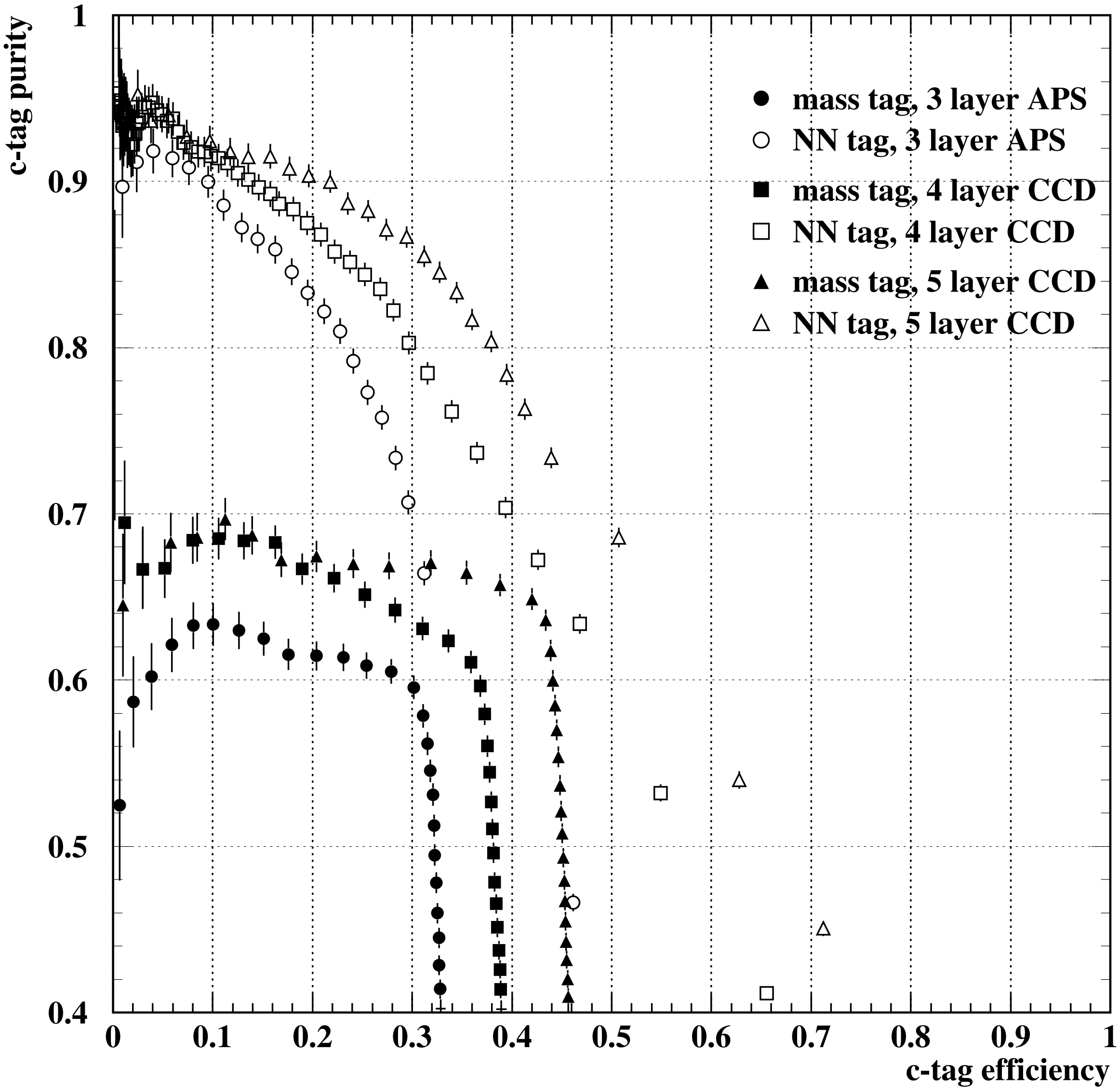

Figure 10: Efficiency *vs.* purity curves for vertex mass and neural network based charm tags with $|\cos\theta| < 0.9$ and different vertex detector options. The initial sample has the Z^0 flavour composition.

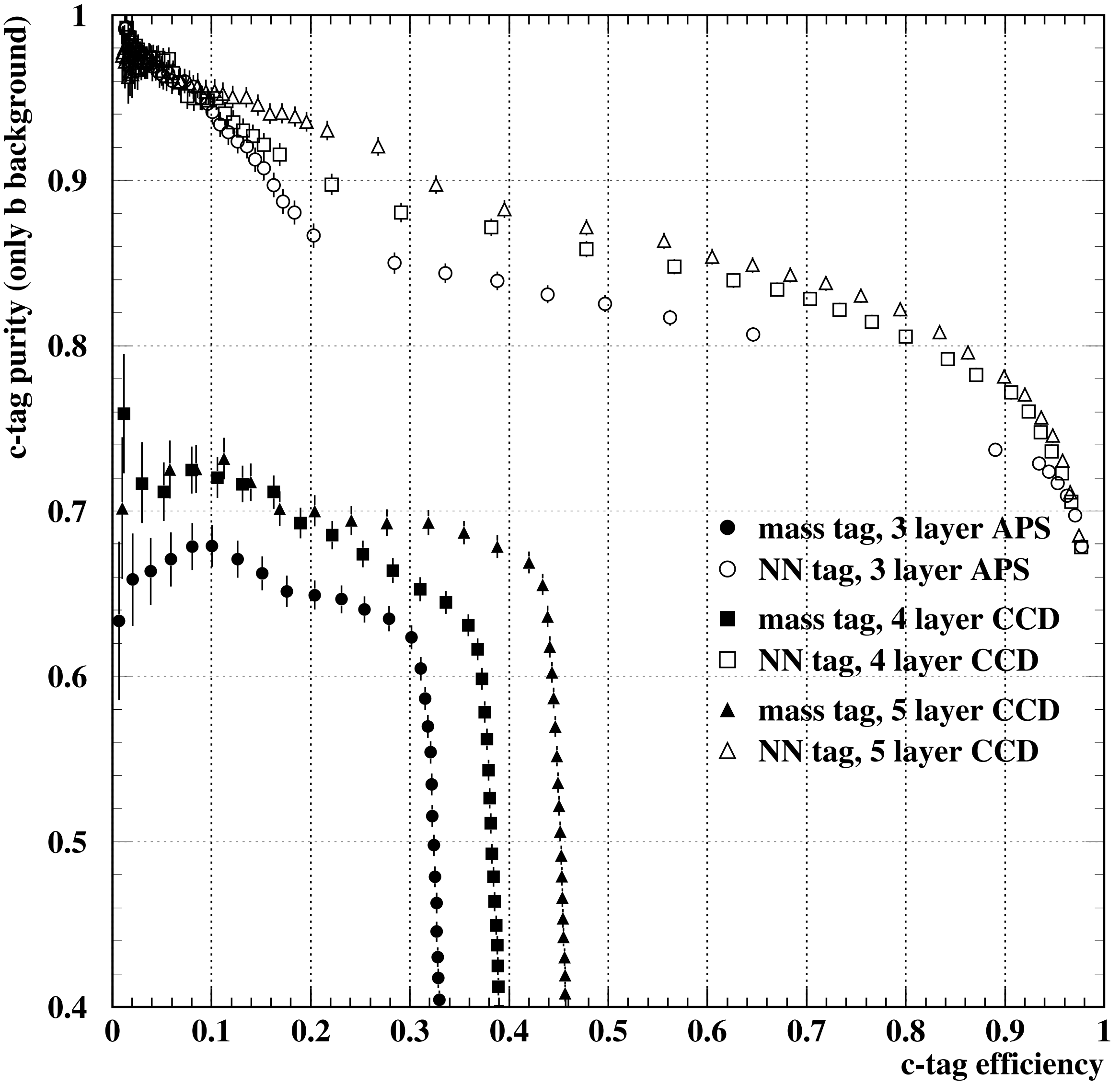

Figure 11: Efficiency *vs.* purity curves for vertex mass and neural network based charm *vs.* bottom tags with $|\cos\theta| < 0.9$ and different vertex detector options. The initial sample is 44 % pure in charm decays.

tagging purity, since the 'natural' event flavour mix can change with energy.

The tagging performance clearly deteriorates significantly with increasing jet energy, in contrast to naive expectations which would suggest a constant or increasing performance. Several contributory factors can be identified:

- The performance of the impact parameter joint probability tag decreases—*e.g.* the purity of a 40 % efficient b-tag based on $P_J(r\phi)$ decreases from 84 % at 45 GeV to 72 % at 300 GeV (with equal initial numbers of u,d,s,c and b jets). The main reason is that more uds jets are classified as unlikely to come from a single vertex at high energy—as the average track multiplicity increases, the probability to get one badly measured track spoiling the P_J value increases.

- The b-tagging performance of the ZVTOP algorithm also decreases at very high jet energies, as a greater fraction of b events are classified as having only one vertex, despite the separation between primary and secondary vertices increasing with b hadron energy. This results in the 'knee' in the b-tagging purity *vs.* efficiency curve visible in Figure 7 moving from 60 % efficiency at 45 GeV to 40 % efficiency at 300 GeV. The main reason for this is that at high energy, many b hadrons travel a long way before decaying—for 300 GeV jets the mean decay distance is 2 cm—well inside the vertex detector itself. The current version of ZVTOP is not well suited to reconstructing such long decay lengths, and has little efficiency for finding b hadrons which decay more than 3 cm from the origin. The track impact parameter and other cuts may need reoptimising for higher energy jets, and the impact parameter resolution for tracks missing several vertex detector hits is obviously degraded.

- The neural networks give differing weights to the different inputs to get the optimum separation, and may need to be retrained for higher energy jets. Similarly, they should be retrained if the relative fractions of the different background quark flavours change.

It is clear that much work remains to be done in optimising the tag performance for higher energies—both in terms of tuning the algorithm parameters and retraining the neural networks if appropriate. By these means it should be possible to improve the performance at high energies beyond what is shown in Figure 12.

The tagging efficiencies shown in Figure 12 have been parameterised and implemented in a FORTRAN subroutine which can be used in physics studies. This subroutine is described in Appendix B.

4 Layout optimisation

The preceding section demonstrated the excellent bottom and charm tagging performance achievable with a neural network based tagging algorithm, and also showed the dependence of the performance on the vertex detector choice. In this section, some more layout studies are described, in particular the effect of the beampipe radius on the tagging performance, and the optimisation of the forward region at high $|\cos\theta|$.

4.1 First layer radius

The vertex detector performance depends strongly on the radius of the first layer (see *e.g.* Figures 4 and 10), and hence on the radius of the beampipe, which must come between the

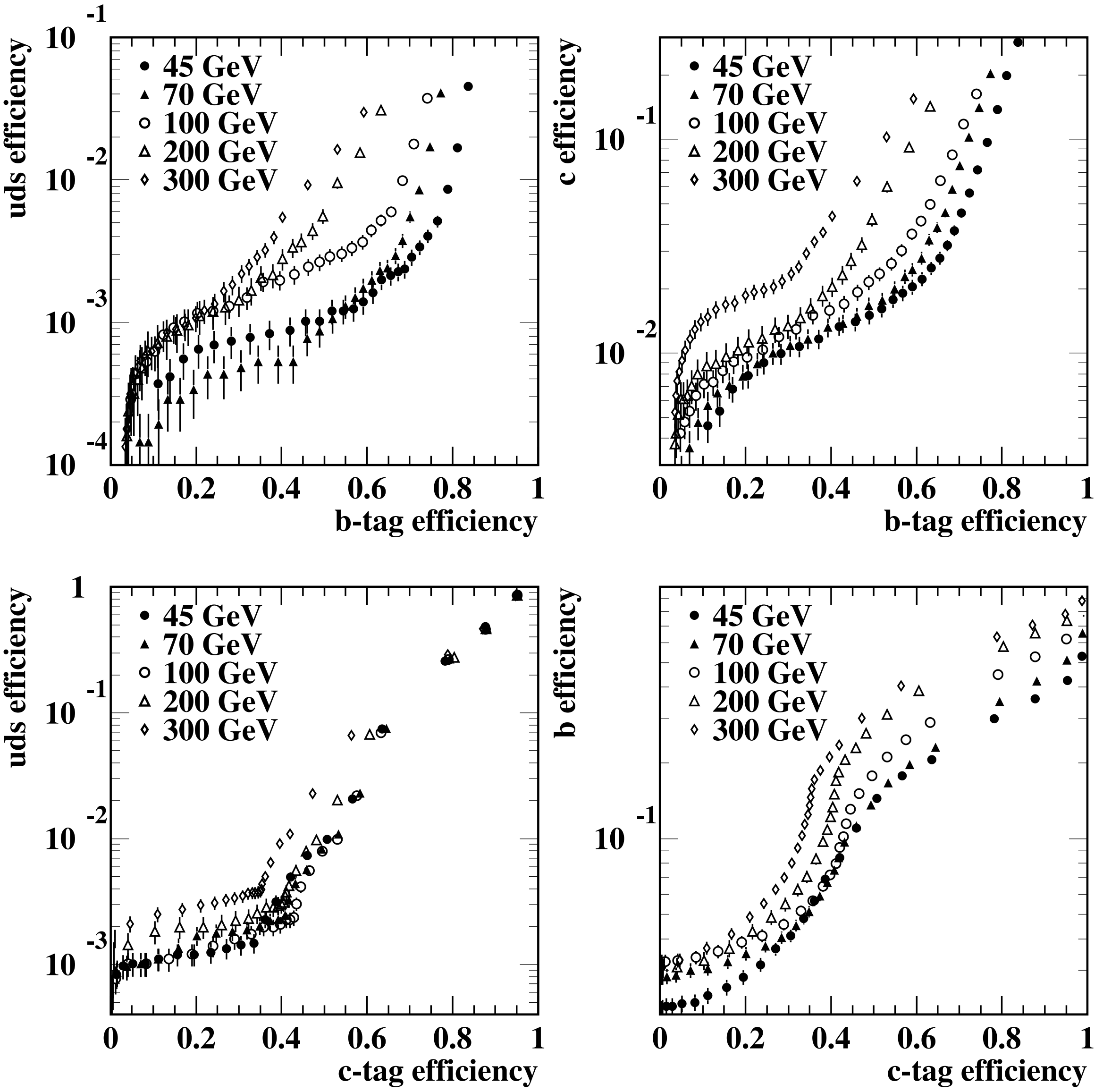

Figure 12: Tagging performance for jets of different energies: uds and c efficiency as a function b efficiency for the b-tagging neural network trained on Z^0 decays (top); uds and b efficiency as a function of c-tagging efficiency for the c-tagging neural network trained on Z^0 decays (bottom).

first detector layer and the beam itself. The best performance is achieved with the beampipe at $r = 1.0\,\mathrm{cm}$, corresponding to a first active layer at $r = 1.2\,\mathrm{cm}$. For comparison, simulations were also done with an alternative 5 layer layout, having the beampipe at $r = 1.5\,\mathrm{cm}$ and the first layer at $r = 1.7\,\mathrm{cm}$, the other layers being left in the same positions (r =2.4, 3.6, 4.8, 6.0 cm). The charm tagging performance is shown for both these layouts, together with the 4 layer layout with the beampipe at $r = 2.0\,\mathrm{cm}$ and the first layer at $r = 2.4\,\mathrm{cm}$, in Figure 13. A small but significant loss in performance of typically 10–15 % is seen on moving the beampipe radius from 1.0–1.5 cm.

The loss in physics performance associated with an increase in the beampipe radius is difficult to quantify, as the charm tagging performance is just one of many limiting factors, though it is particularly important in multiple tagged jet topologies. However, a $r = 1.0\,\mathrm{cm}$ beampipe puts severe constraints on the accelerator interaction region, particularly for the collimation system. Therefore it has been decided to adopt $r = 1.4\,\mathrm{cm}$ as the beampipe radius for the baseline detector in the linear collider TDR [15].

4.2 Forward region

In the 5 layer CCD vertex detector layout (see Figure 2), both the first and fifth layers have polar angle coverage only up to $|\cos\theta| = 0.9$. The small number of vertex detector hits in the region $0.9 < |\cos\theta| < 0.98$ leads to a much reduced impact parameter resolution, in addition to the degradation caused by traversing the CCD layers at small incident angles.

One possible way to improve the forward coverage of the CCD vertex detector is to add 'endwheels' or discs of pixels at the ends of the detector—similar to the cones in the APS detector layout (Figure 3). This idea was explored by adding two discs at $z = 14\,\mathrm{cm}$ and $z = 15.5$, each extending from $r = 2.4\mathrm{cm}$ to $r = 6.0\,\mathrm{cm}$, and having the same point resolution as the barrel detectors ($3.5\,\mu$m). This addition results in an extra two hits per track in the range $0.9 < |\cos\theta| < 0.98$. However, the improvement in impact parameter resolution and tagging performance is very small, since the extra layers are more than 15 cm from the interaction point and the first material (the beampipe). Hence such endwheels are not a promising way to increase the forward region performance.

To make a significant improvement in the forward region, additional measurement points are required close to the beam. In the current design, the first CCD layer extends only to $z = 2.5\,\mathrm{cm}$, motivated by concerns about the background level, primarily e^+e^- pairs produced from beamstrahlung photons. At a fixed radius, the background level is expected to be small at $z = 0$, but increase rapidly at z values of a few cm. However, recent calculations of the background level [16], reproduced in Figure 14, show that the 'safe' region extends beyond $z = 5\,\mathrm{cm}$ even at $r = 1.2\,\mathrm{cm}$. Therefore it may be possible to extend the first vertex layer beyond the $z = 2.5\,\mathrm{cm}$ limit in the current design.

To study the possible gain in charm tagging performance, an alternative layout was implemented, where the active area of the first vertex layer was doubled in length to $z = 5\,\mathrm{cm}$. The electronics was placed beyond it as in Figure 2, and the position of the beampipe flare was also moved by 2.5cm in z to accommodate the modified detector. All other vertex detector layers remained the same. The performance gain was quantified by studying the charm tag efficiency at fixed purity, as a function of the jet polar angle θ. The results are shown in Figure 15, for high and low charm tag purities (0.7 and 0.4) in Z^0 decays. The tagging efficiency is relatively constant for $|\theta| > 0.6$ ($|\cos\theta| < 0.83$), but deteriorates rapidly beyond this point. The layout with extended first layer shows a clear improvement—the charm tagging

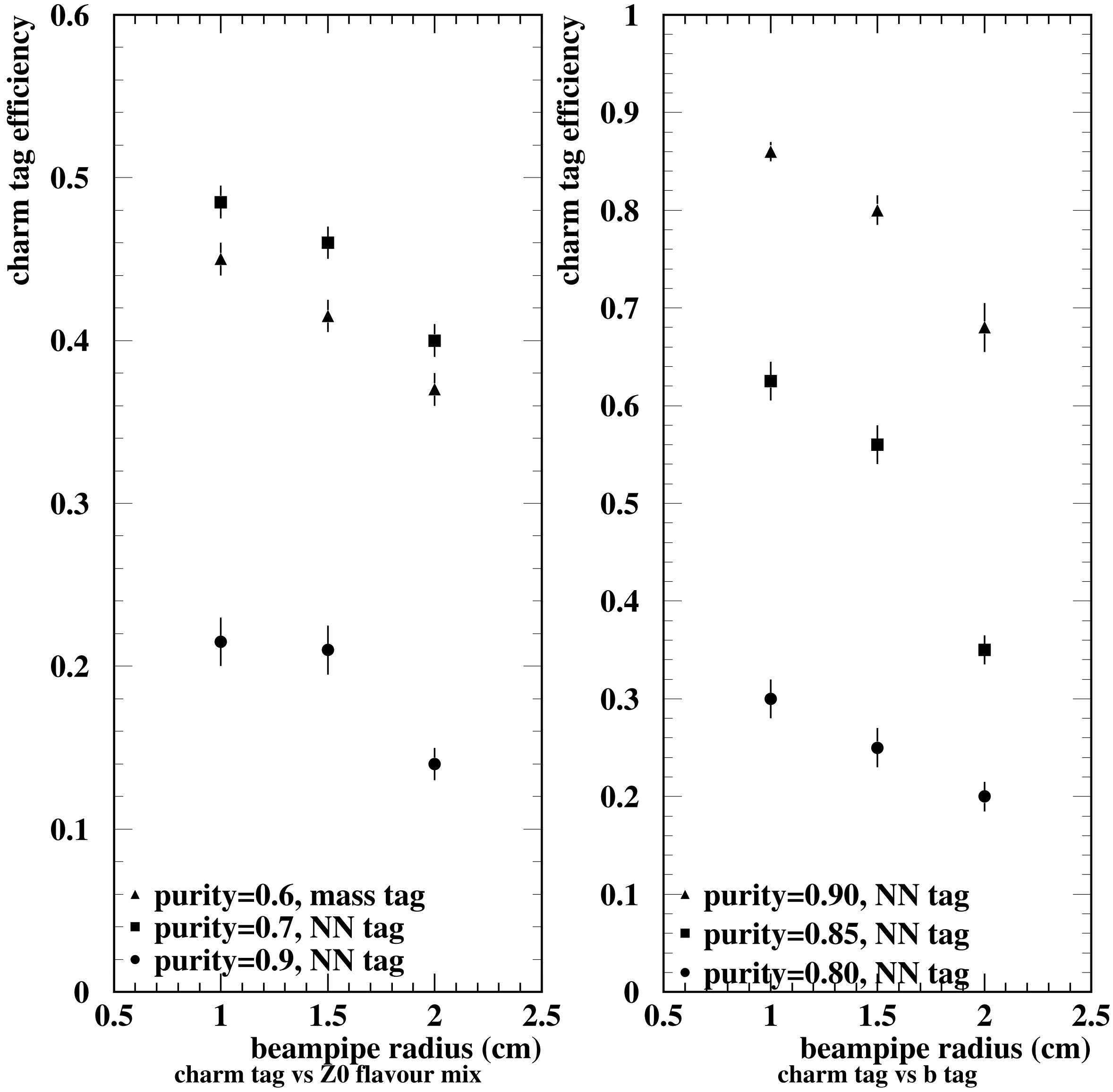

Figure 13: Charm jet tagging efficiency *vs.* beampipe radius at various tagging purities. The left plot shows charm tagging in Z^0 events, the right plot only b *vs.* c separation.

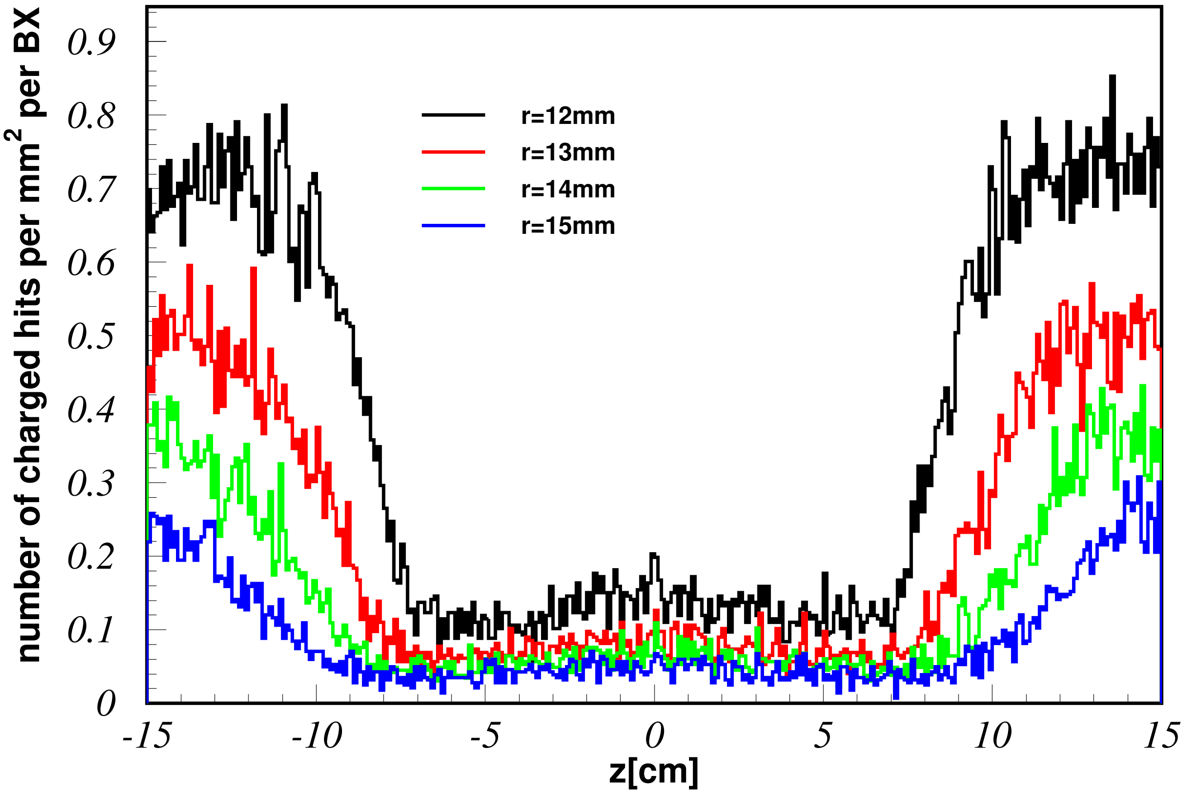

Figure 14: Background hit density per bunch crossing from e^+e^- pairs in the vertex detector region, for a solenoid magnetic field of $B = 3\,\mathrm{T}$ [16].

efficiency being two or three times greater than for the standard design. It remains to be seen how important this gain is for particular physics analyses, but it is clear that first layer should be as long as possible to maximise the tagging performance, as long as background from beamstrahlung pairs does not begin to compromise the performance.

5 Pattern recognition studies

The above studies have all been done using 'perfect' pattern recognition—tracks have been reconstructed by using the GEANT truth (KINE) information to collect all detector hits belonging to a particular charged particle. The DELFIT package included in BRAHMS [5] has then been used to fit the track, discarding any hits which do not fit well, due to *e.g.* material interactions in the detector.

However, in the real detector full pattern recognition will be required, and the level of incorrect hit assignments and ambiguities may well have an influence on the performance of the vertex detector. In current experiments *e.g.* at LEP, track pattern recognition is performed first in the large central tracking detectors (corresponding to the TPC in the case of the linear collider detector), and the resulting track segments are extrapolated inwards to the vertex detector layers. This strategy was motivated by the small number of layers,

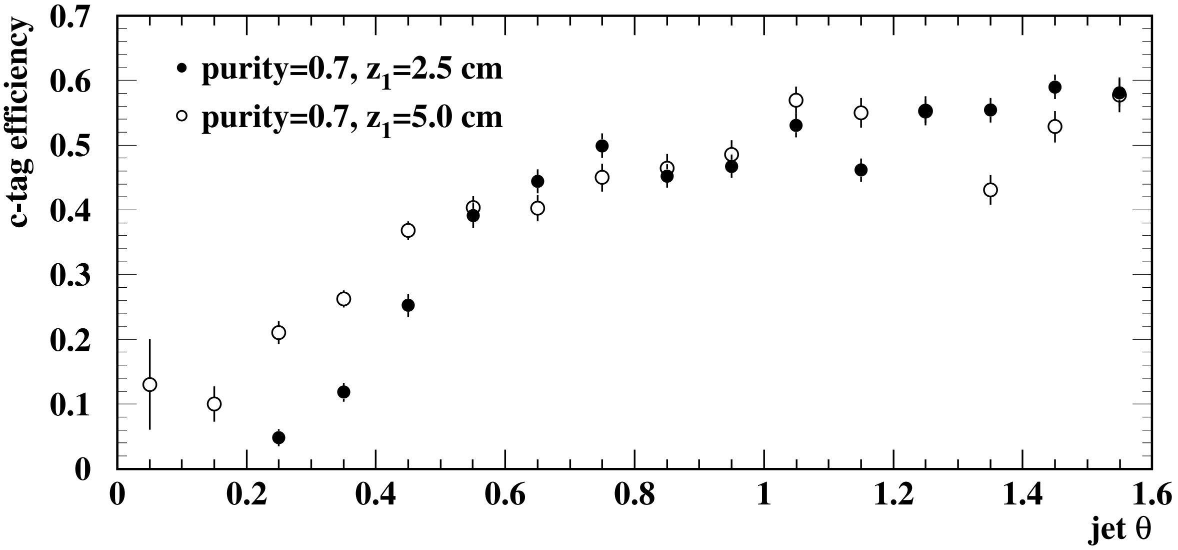

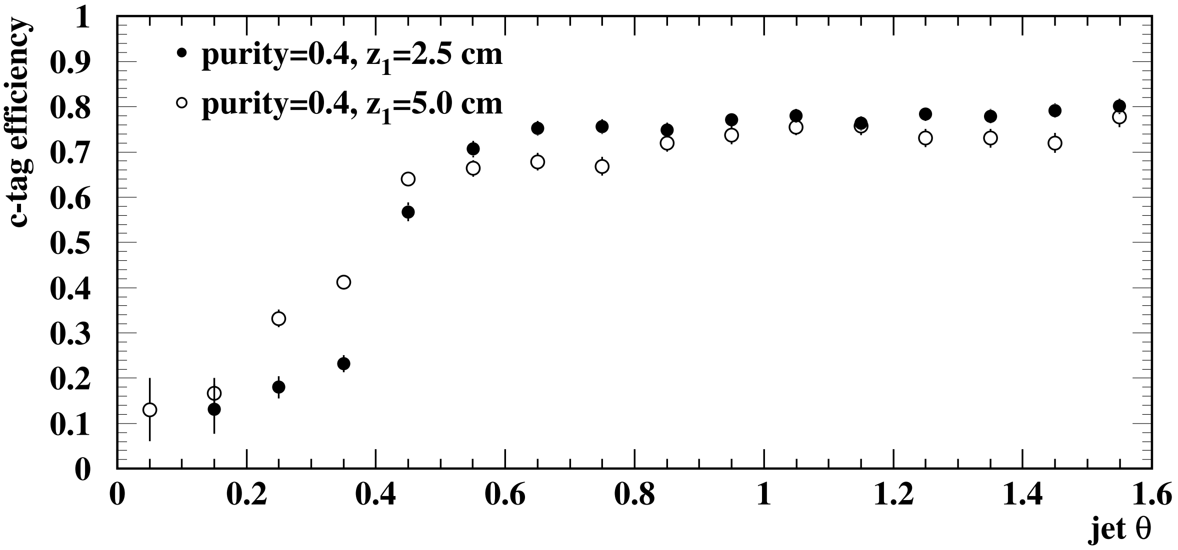

Figure 15: Charm tagging efficiency in Z^0 decays as a function of jet polar angle θ, for two different tag purities and vertex detector layer 1 half-lengths z_1.

typically with only r-ϕ coordinate readout, of the first silicon microvertex detectors. However, the 5 layer CCD pixel detector proposed for the linear collider has full 3D readout, extremely high granularity and enough layers to perform robust standalone pattern recognition. This possibility may allow a rather different global pattern recognition strategy in which the vertex detector participates at an equal level to the TPC in finding track segments to initiate a full track search. Such a scheme has already been used successfully by DELPHI with their high performance 3 layer vertex detector [17]. The possibility to do standalone vertex detector track finding also offers obvious advantages for the initial running in and alignment of the detector. A simple vertex detector standalone pattern recognition algorithm has therefore been implemented within the BRAHMS framework, to evaluate the possible performance, the influence of background and the potential contribution of the vertex detector to the overall track pattern recognition. All studies in this section have been performed with the default 5 layer CCD vertex detector shown in Figure 2.

5.1 Pattern recognition algorithm

The vertex detector pattern recognition algorithm is described below. The algorithm is rather simplistic, and is based on a combinatoric search of hit combinations that may make a track. This algorithm uses essentially all the available information, but is very CPU intensive in the presence of large numbers of background or noise hits. However, the main purpose of this study is to evaluate the possible vertex detector performance, not to produce a viable pattern recognition algorithm for the real detector—the latter would require much more work and detailed performance tuning.

The algorithm proceeds in several steps:

- The vertex detector is divided into sectors in ϕ and $\cos\theta$, typically $64 \times 64 = 4096$ sectors. This reduces the number of hit combinations to be considered—tracks will only be found if they have hits in at most 2 different ϕ and 2 different $\cos\theta$ sectors. Very low momentum tracks with large curvature will not be found, as they will span more than 2 ϕ sectors, with 64 ϕ sectors in total, this reduces the efficiency for tracks below about 200 MeV.

- Each 2×2 'window' of adjacent sectors is then considered in turn. A track candidate is formed by taking a hit from each layer of the vertex detector, and attempting to fit a track through all 5 selected hits. The fit is done separately in the two coordinate planes—a circle fit in r-ϕ and a straight line in s-z, where s is the track arc length. No account is taken of multiple scattering or energy loss in the vertex detector layers, which causes a slight inefficiency for low momentum tracks. The track candidate is accepted if it has r-ϕ and s-z χ^2 of less than 5 per degree of freedom and impact parameters with respect to the nominal interaction point of less than 5 mm in r-ϕ and r-z.

- The track candidate fit is repeated for all possible 5 hit combinations in the sector window, and all acceptable candidates are stored. Some optimisations are applied to speed up the algorithm—*e.g.* a combination of 3 hits from layers 3, 4 and 5 which already has a very bad s-z χ^2 is discarded immediately, without adding all the possible combinations of hits in layers 1 and 2.

- The stored track candidates are sorted by increasing χ^2, and the first is output as a found track. The hits belonging to this track are marked as used, and any other track candidates sharing these hits are discarded[1]. The process continues until all track candidates in the sector window have been output or discarded.

- The algorithm moves onto the next sector window and the track finding process is repeated. Hits marked as used in a previous sector window are not considered again, so tracks which are fully contained in a single sector are not found more than once.
- When all sector windows have been processed, the entire algorithm is repeated, this time looking for 4 hit tracks, where the hit in one layer is missing. This allows for some vertex detector inefficiency, and for some tracks with material interactions to be recovered.

The final output of the algorithm is a list of tracks, each with associated track parameters and error matrix from the track fit, and corresponding list of hits.

5.2 Pattern recognition performance

The performance of the pattern recognition algorithm was initially evaluated using samples of Z^0 decays. Three performance measures were used:

Trackfinding efficiency defined as the fraction of true tracks which were reconstructed with 4 or more hits from the correct track.

Spoiled track fraction defined as the fraction of true tracks which were reconstructed but with one truth hit missing or replaced by a hit from another track or background. These tracks are included in the efficiency defined above, the difference between the efficiency and the spoiled track fraction gives the fraction of tracks reconstructed perfectly with 5 correct hits.

Fake track rate defined as the number of tracks per event which have 3 or less hits from a unique truth track. Such tracks arise from combinations of hits from different tracks, background or both.

All these measures can be evaluated as a function of track transverse momentum p_t and polar angle $\cos\theta$.

The algorithm was first tested with a sample of Z^0 decays simulated with all GEANT processes except $d\mathrm{E}/d\mathrm{x}$ energy loss switched off. This avoids any tracks being lost due to multiple scattering, material interactions *etc.* The resulting trackfinding efficiencies and spoiled track fractions are shown as the solid circles in Figure 16. The track finding efficiency is essentially 100 % except at very low momentum (where the track cross more than two ϕ sectors) and at polar angles of $|\cos\theta| > 0.9$, where the vertex detector coverage ends. The spoiled track fraction is also very low, and the spoiled tracks are concentrated at low p_t.

The results with all interactions switched on (corresponding to full GEANT simulation) are shown in Figure 16 as the open circles. The efficiency is again very close to 100 %, except below $p_t = 1\,\mathrm{GeV}$ where energy loss and multiple scattering become important. Using a Billoir fit (which accounts for these processes) instead of the simple circle fit improves the performance in this region, at the expense of longer execution time.

[1] In the version of the algorithm to be released in BRAHMS as part of the global pattern recognition program, track candidates are allowed to share hits, as such ambiguities are resolved in a later stage, also using information from other subdetectors.

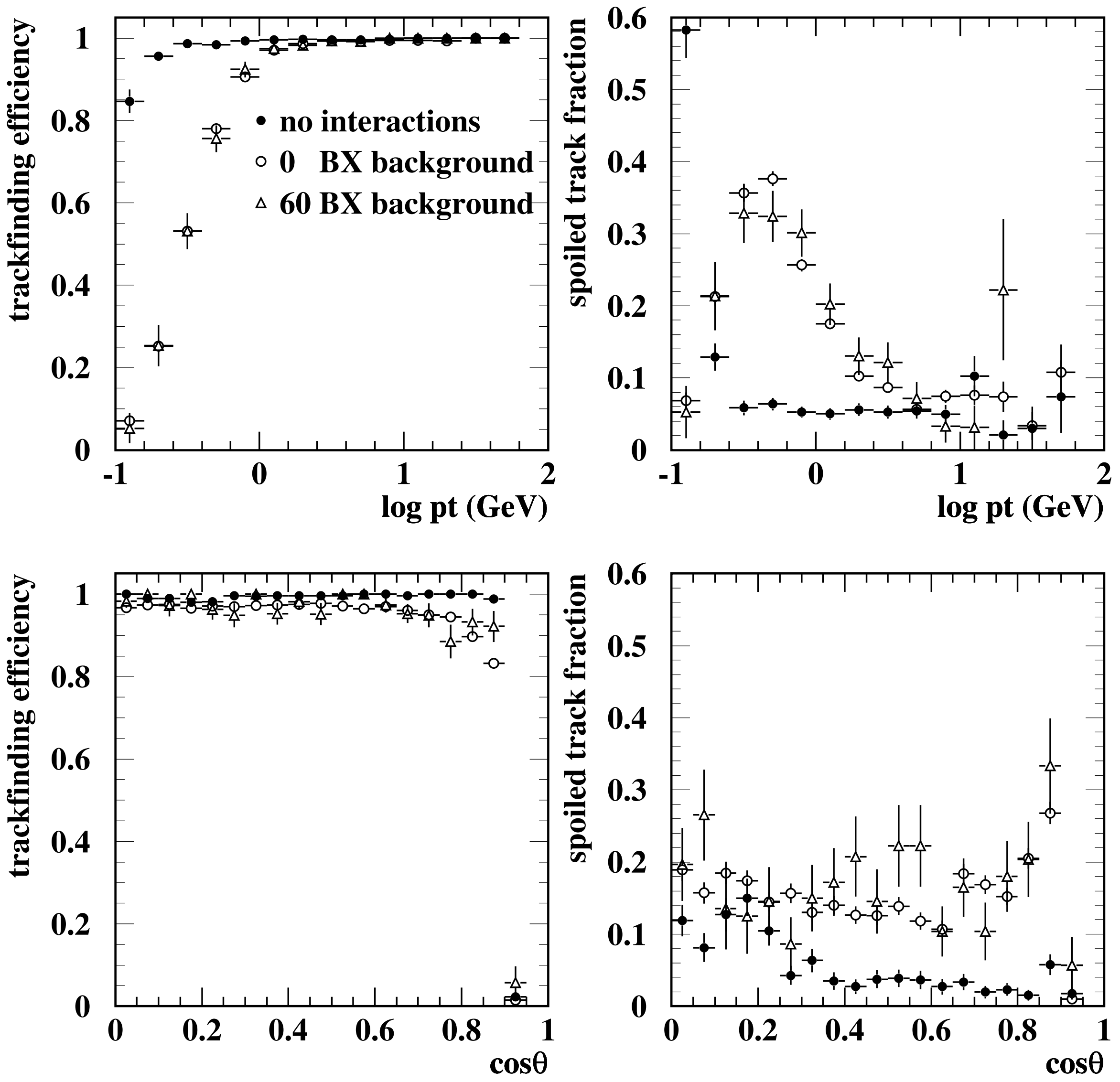

Figure 16: Standalone vertex detector pattern recognition performance in Z^0 decays: track finding efficiency and spoiled track fractions with (1) no GEANT material interactions and no beamstrahlung background, (2) full GEANT material interactions and no beamstrahlung background and (3) full GEANT material interactions and 60 bunch crossings of beam-strahlung background, corresponding to full design luminosity.

Layer	Radius (cm)	Hits per bunch crossing	
		$B = 3\,\mathrm{T}$	$B = 4\,\mathrm{T}$
1	1.2	690	334
2	2.4	431	202
3	3.6	128	79
4	4.8	52	37
5	6.0	19	6

Table 3: Expected number of hits from charged particles on each layer of the CCD vertex detector per bunch crossing (BX), for solenoid magnetic fields of 3 and 4 T [19].

A major issue for the CCD vertex detector is that of occupancy due to machine backgrounds. The process of 'clocking' the pixel data along the rows and columns means that the data from the physics event of interest is contaminated by many overlapping hits from different bunch crossings. Using a 'column parallel' readout scheme, the entire detector can be read out in $25\,\mu$s, giving around 60 bunch crossings of superimposed background [18]. The expected numbers of charged hits per bunch crossing from beamstrahlung background are given in Table 3 [19]. Since most of the e^+e^- pairs from beamstrahlung photons have very low transverse momentum, the number of hits is much larger in the inner layers, and also decreases with a stronger solenoid field. The results discussed here have been produced assuming the higher background associated with a 3 T magnetic field.

The occupancy from beamstrahlung background was simulated by adding the appropriate number of hits on each vertex detector layer (*i.e.* $60 \times 690 = 41400$ extra hits on layer 1 for 60 bunch crossings of background.) The hit positions were distributed randomly, uniformly in $\cos\theta$ and ϕ, as the background is reasonably constant as a function of z within the vertex detector region (see Figure 14). The pattern recognition was then run including these extra hits. The effects on the track finding efficiency and spoiled track rates are shown by the open triangles in Figure 16, and can be seen to be small, the performance being largely unaffected by the background occupancy.

The jets produced in Z^0 decays are typical of those expected in more complex multi-jet final states. In general these will be separated in angle and occupy different regions of the vertex detector. Hence the pattern recognition should be able to cope with such multi-jet events. A more extreme and difficult case is provided by $e^+e^- \to \tau^+\tau^-$ events at a high centre of mass energy of $\sqrt{s} = 800\,\mathrm{GeV}$. The tau decays give rise to very collimated low multiplicity jets, in which the tracks are very close together. Additionally, the 400 GeV taus travel on average 20 mm from the interaction point before decaying, so some fraction decay between the inner layers of the vertex detector, leading to more 'spoiled' tracks with hits missing in the innermost layer.

To study this, three sets of $\tau^+\tau^-$ events were generated as for the Z^0 decays discussed above, with no material interactions, interactions but no background, and 60 bunch crossings of background. The pattern recognition performance is shown in Figure 17, which can be compared with Figure 16. The track finding efficiency is again very good, and not significantly affected by interactions or beamstrahlung background. Around 30 % of tracks are 'spoiled' with no hit on the first vertex detector layer, due to τ decays between the first and second layers. However, this number is not significantly increased by background. These results show that the standalone vertex detector pattern recognition can function even in the difficult

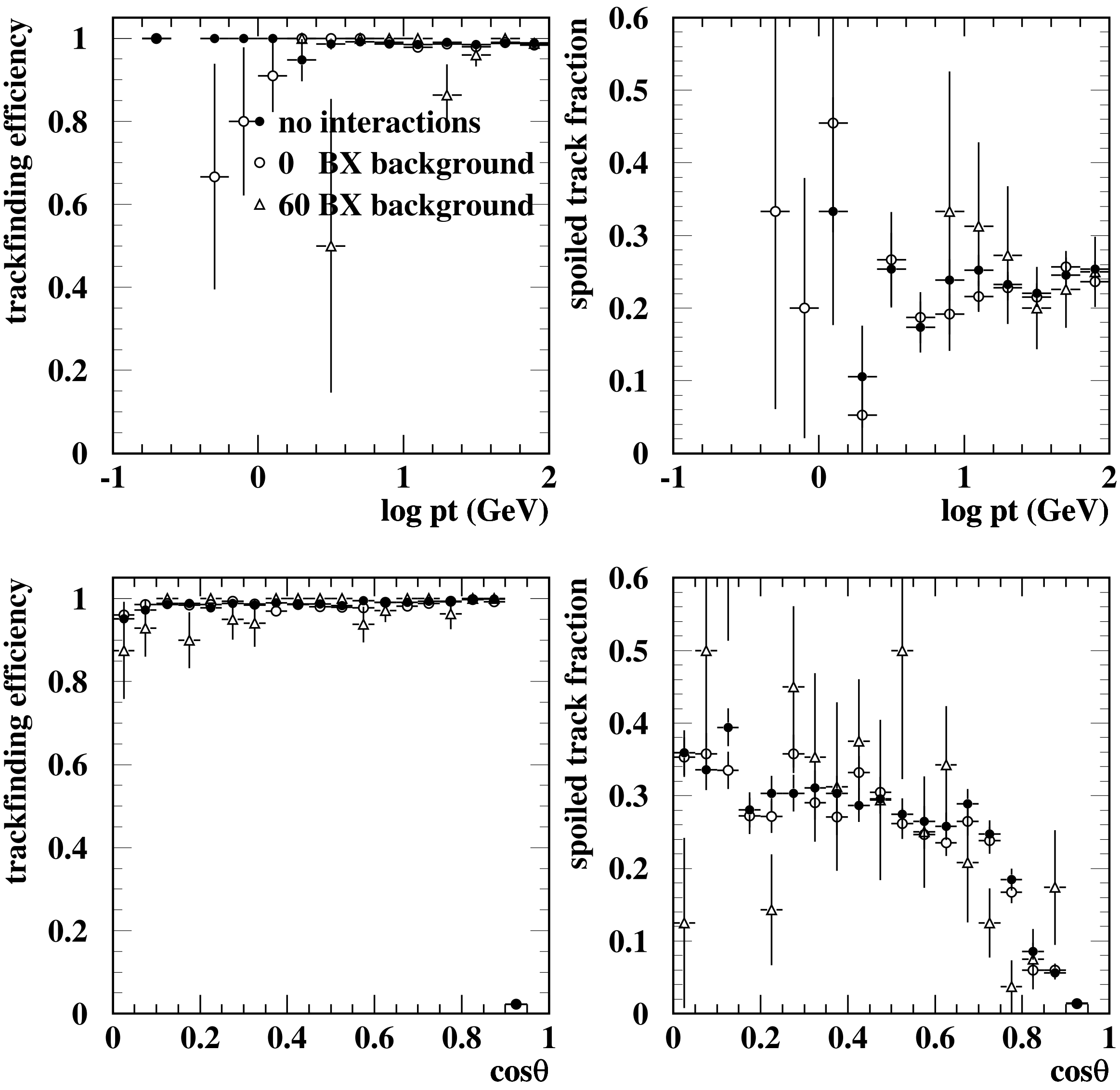

Figure 17: Standalone vertex detector pattern recognition performance in $e^+e^- \to \tau^+\tau^-$ events at $\sqrt{s} = 800\,\mathrm{GeV}$: track finding efficiency and spoiled track fractions with (1) no GEANT material interactions and no beamstrahlung background, (2) full GEANT material interactions and no beamstrahlung background and (3) full GEANT material interactions and 60 bunch crossings of beamstrahlung background, corresponding to full design luminosity.

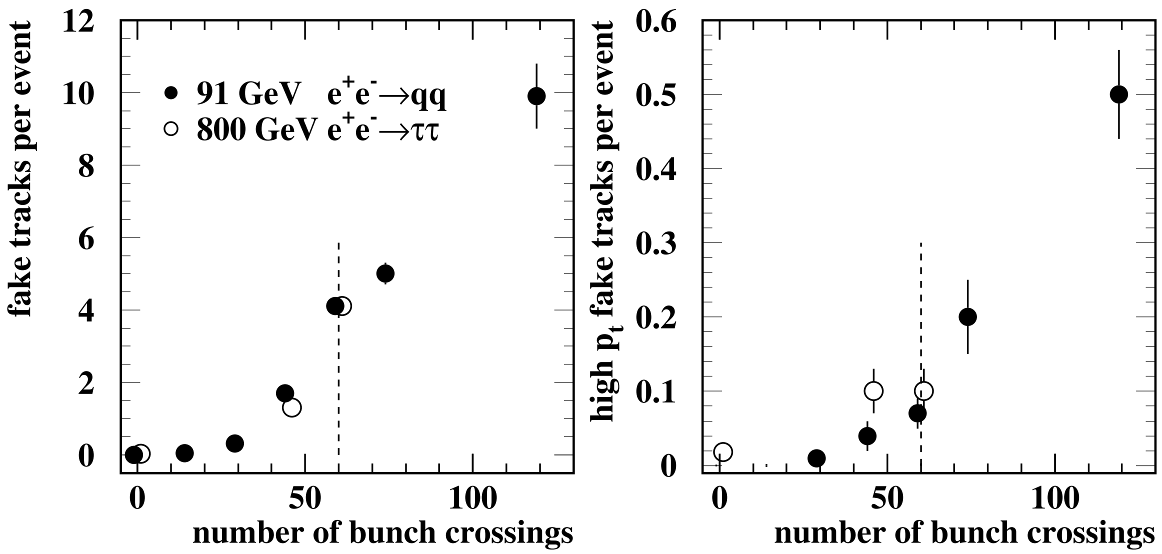

Figure 18: Expected number of fake tracks per event as a function of the number of superimposed bunch crossings of beamstrahlung background, for $e^+e^- Z^0 \to q\overline{q}$ events at $\sqrt{s} = 91\,\mathrm{GeV}$ (solid points) and $e^+e^- \to \tau^+\tau^-$ events at $\sqrt{s} = 800\,\mathrm{GeV}$ (open points). The total rate of fake tracks is shown on the left plot, and the rate of fake tracks having $p_t > 1\,\mathrm{GeV}$ and $|\cos\theta| < 0.8$ on the right plot.

environment of high energy τ decays, where the other tracking detectors may have problems.

5.3 Fake track rates

As well as the ability to find the true tracks correctly, discussed above, it is also important that the rate of reconstructed fake tracks is low. The number of fake tracks per event (defined as discussed in Section 5.2) was determined as a function of the number of bunch crossings of superimposed beamstrahlung background. The results are shown in Figure 18, for both $Z^0 \to q\overline{q}$ and 800 GeV $\tau\tau$ events. The fake track rate is negligible without background, but rises to around 4 tracks per event at the nominal background level, and 10 tracks per event at twice this level (120 bunch crossings). The rates are similar for both types of physics event. These results have been obtained for a 3 T magnetic field, and the rates for a 4 T field will be lower due to the smaller background occupancy (see Table 3).

Most of the reconstructed fake tracks have low p_t (below 1 GeV) and are at high polar angles beyond $|\cos\theta| = 0.8$, where the vertex detector resolution is poorest. Such tracks should not be a problem for the global pattern recognition, as they are unlikely to match any tracks found in the other detectors. The most dangerous fake tracks are those with $p_t > 1\,\mathrm{GeV}$ and $|\cos\theta| < 0.8$, *i.e.* in the central detector region, and the rate of such reconstructed fake tracks is also shown in Figure 18. Around 0.1 fake track per event is found with 60 bunch crossings, rising to around 0.5 with 120 bunch crossings. Again, these fake track levels should be manageable, and will be lower with a 4 T magnetic field.

5.4 Track parameter reconstruction

It is also of interest to compare the track parameter resolutions obtained with the vertex detector alone with those from the whole tracking system. The track parameter resolutions were measured as a function of p_t for single pions in the range $0.5 < p < 10\,\text{GeV}$ and $|\cos\theta| < 0.9$, using the track parameters determined by the vertex detector standalone pattern recognition, and by the full track fit using information from all subdetectors. The results are shown in Figure 19. For the track curvature $1/p_t$, where the long lever arm of the TPC is important, the vertex detector resolution is very poor, but for the r-ϕ track angle and impact parameter d_0, the vertex detector is within a factor two of the entire tracking detector (the degradation in d_0 resolution results from the coupling of d_0 and the track curvature $1/p_t$). For the track polar angle $\cos\theta$ and r-z plane impact parameter z_0, the vertex detector alone is almost as good as the entire tracking system, as the vertex detector provides easily the most precise track z measurements and sufficient lever arm to measure the polar angle.

These results emphasise the potential of the vertex detector to contribute to the overall pattern recognition—it can reconstruct track segments with high efficiency and low background, and with very precise values for 4 out of 5 track parameters. The ability to match track segments not only in space but in angle should greatly help the global pattern recognition to achieve a small rate of fake or misreconstructed tracks. The usefulness of precise vertex detector standalone tracking for detector calibration and alignment should also be stressed.

The studies in this section have been performed with the 5 layer CCD vertex detector option. Since hits from 3 layers are needed to define a track, 4 layers is the minimum for which any reasonable standalone tracking is possible, and 5 layers provides more background rejection and robustness against missing hits. The arguments in favour of standalone pattern recognition capability therefore suggest a 5 layer detector is very desirable. However, the APS detector option has only 3 layers (see figure 3), and since the detector layers are thicker than for the CCD detector, adding more layers will degrade the performance due to multiple scattering. It has been recently proposed to replace the ITC wire chamber with one or two layers of silicon strip detectors (SIT), and it may be possible to use these layers in conjunction with the APS vertex detector to do standalone pattern recognition in the precision trackers in front of the TPC. However, in this case the advantages for alignment of doing pattern recognition entirely in the vertex detector would be lost.

6 Conclusions

The performance of various vertex detector options for the TESLA linear collider detector has been studied, with particular regard to heavy flavour tagging. Excellent performance can be achieved, far in excess of that at current experiments. A few general points are worth stating:

- Charm tagging is much more sensitive to the vertex detector performance than b-tagging, especially in a background of all five quark flavours. In particular, the radius of the first detector layer (and hence the beampipe) is important, there being a 10–15% deterioration in charm tagging performance per jet as the beampipe radius is moved from 1.0 to 1.5 cm. Similarly, the tagging performance in the forward region benefits much more from increasing the length of the first layer as much as possible than from adding forward endwheel detectors further from the interaction point.

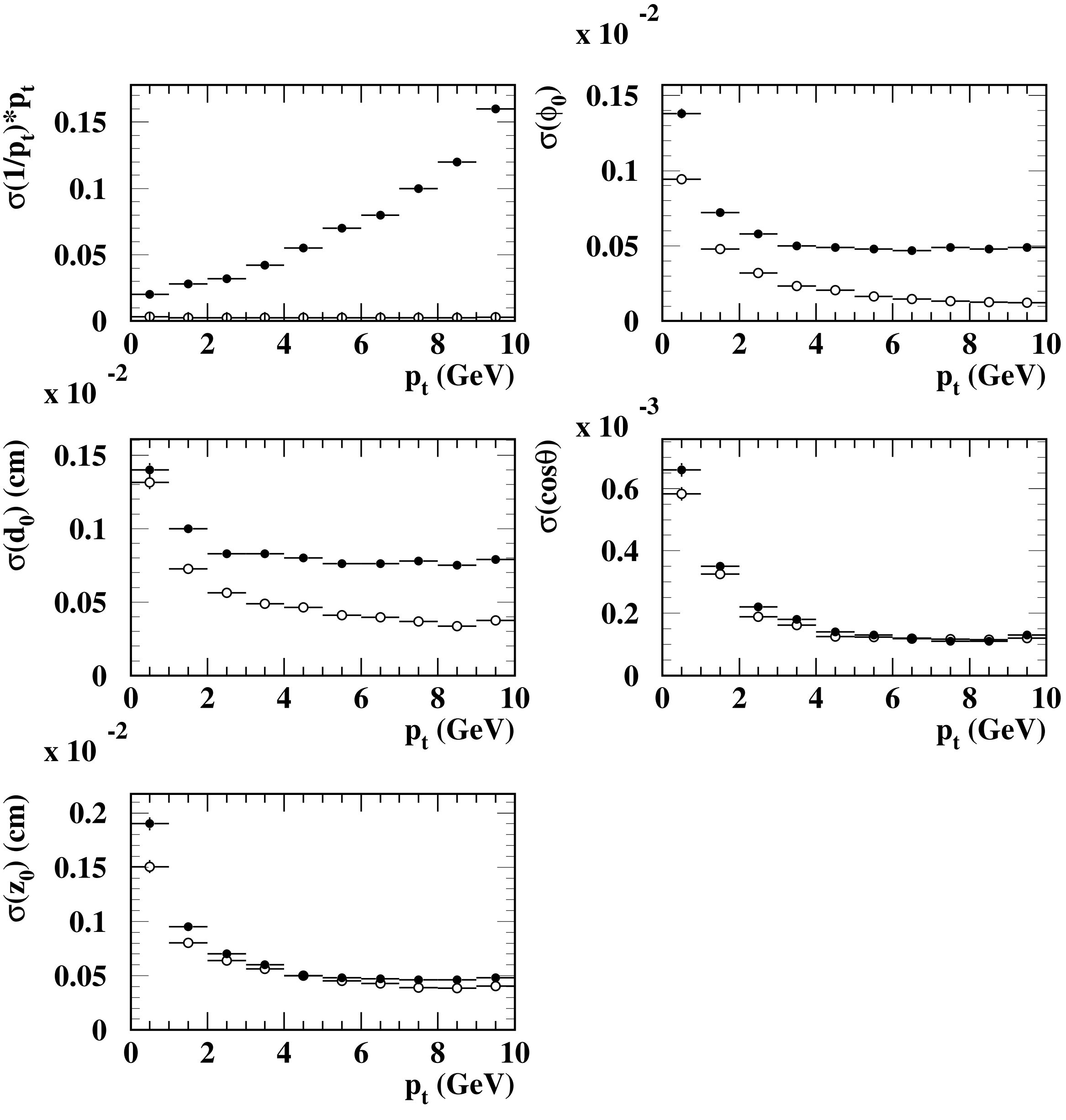

Figure 19: Track parameter resolution for charged pions as a function of p_t for the vertex detector pattern recognition alone (open circles) and the full track fit using information from all subdetectors (filled circles).

- The ZVTOP algorithm from SLD gives excellent b and c tagging performance and fully exploits the resolution of the vertex detector. However, the combination of information from this and other algorithms (*e.g.* in a neural network) is also essential to get the maximum performance, especially for charm tagging. The optimisation of the tagging performance also depends crucially on the exact mixture of background (light and bottom quarks) expected in the selected sample.
- A five layer pixel vertex detector can contribute substantially to the track pattern recognition, due to its excellent three dimensional granularity. Most of the tracks in typical events can be found by the vertex detector alone, and the fake track rates remain tolerable even in the presence of background hits from beamstrahlung processes. This standalone pattern recognition also has considerable advantages for detector commissioning and alignment.

Clearly, much work remains to be done. The algorithms need to be optimised in more detail for different jet energies, and for the final detector layout selected for the TESLA technical design report. Other properties of reconstructed vertices—*e.g.* decay length resolution and secondary vertex charge, may also have an influence on the design. Finally, work on the global pattern recognition scheme, and the role of the vertex detector within it, is only just starting.

☺

Acknowledgements

Many people have contributed to the success of the work described in this note. The author would like to thank in particular David Jackson and Homer Neal for the original ZVTOP vertexing code, Ties Behnke, Grahame Blair, Phil Burrows and Chris Damerell for useful discussions, and Rolf Heuer for buying coffee during the preparation of the note.

☺

Appendix A: Implementation of vertexing code

A public version of the code used to perform these studies has been made available for use with the simulation program BRAHMS. It should be made available in a future release of BRAHMS, alternatively contact `richard.hawkings@cern.ch` for a copy. This appendix describes some technical details of the code and some guide to its use.

The code comprises two separate files: `bvreco.car` and `vxuser.car`. The former provides a library of reconstruction and vertexing routines. The latter is a simple user 'main program' to replace the BRAHMS user code `bruser.car` and shows how to call the routines and fill a simple b/c tagging ntuple, similar to the one used to perform the studies described in this note. The vertex detector pattern recognition code discussed in Section 5 is not included, but will be released separately as part of the overall BRAHMS pattern recognition software.

The `bvreco.car` file is structured into several patches, as follows:

Patch BVCDES: This contains all the common block definitions for the reconstruction and vertexing code. In particular, the decision has been taken to make all the code operate from a set of common blocks containing the 'reconstructed event'—playing the role of a 'mini-DST', which is separate from the output of BRAHMS. Thus the tracks are stored in the LCTRK common, the 'energy flow' objects in LCEVNT and so on. This allows the code to be used outside of the BRAHMS simulation—for example reading the necessary information from an DST-ntuple, or from a fast Monte Carlo such as SIMDET. [2]

The track parameters are stored using the OPAL track parameter convention (κ, ϕ_0, d_0, $\tan\lambda$, z_0) rather than the DELPHI one used in CHGTRAK, and are converted during the common block filling. This allows various OPAL library routines for vertex finding to be employed, and also takes advantage of the existence of a version of ZVTOP using the OPAL track parameter conventions.

Patch BVRECN: This provides basic 'event reconstruction' code, and performs two distinct functions—filling the LCTRK and LCEVNT common blocks described above from the BRAHMS CHGTRAK track common block, and providing basic event reconstruction tools—jet and thrust finding, primary vertex reconstruction and event acceptance cuts. The jet and thrust finding routines have been taken from the OPAL PX library, and the primary vertex algorithm is modelled on the OPAL one (see Section 2.2). These functions, and the jet finding parameters, are switchable using FFREAD datacards defined during initialisation in the routine BRINIT.

Patch BVBTAG: This provides the core vertexing routines, and includes code to implement all of the vertexing algorithms discussed in this note. The code is structured such that a single call to the subroutine BVBCTG will provide all the tagging variables (including the neural network outputs) for a particular jet, defined previously with the jetfinding code. The individual algorithms are also available to be called separately, if needed. The actual neural network implementations are included in the subroutine BVTNNV.

Patch BVZTOP: This provides the ZVTOP vertexing package itself, apart from the interface routine, which is in the patch BVBTAG. This code has a complicated history, having started life as the original ZVTOP algorithm written in SLD MORTRAN by David Jackson, then being converted to FORTRAN 77 and OPAL track parameters by Homer Neal, and finally being interfaced to the BRAHMS code by the present author. Internally, the code still uses SLD track parameters in some places—conversions being done to and from OPAL parameters where necessary. It is rather complex, but can be treated as a 'black box' by most users.

Patch BVUTIL: This patch contains general utility routines, *e.g.* a subroutine to convert between DELPHI and OPAL track parameters.

Patch BVOPUT: This patch contains all the routines that have been taken from the OPAL PX (general physics utilities, jet and thrust finding), BT (b-tagging and vertex reconstruction) and OU (track and vertex fitting) libraries. Some of them have been modified for the linear collider environment.

In order to use this code, the user has to call the initialisation routines BRINIT and BVINIT from UBINIT, and BRSETR and BVSETR from UBSETR. Then the event reconstruction routine BRECON needs to be called from UBOUT, followed by whatever vertex reconstruction and tagging routines are required.

[2] Unfortunately, the current version of SIMDET provides no track error matrices, so cannot easily be used as an input to the vertexing code.

The example program `vxuser.car` shows how this is done, and also provides a simple interface for the PYTHIA 6.1 event generator [3] [6]. The code contains the following patches:

Patch VXCDES: This patch contains the common blocks for overall steering of the program and defining the (column wise) ntuple.

Patch PYCMMN: This patch contains definitions of the PYTHIA 6.1 common blocks.

Patch VXCODE: This patch contains the user code, including definitions of all the standard BRAHMS user subroutines, and the booking and filling of an ntuple containing vertexing information. The vertex tagging algorithms are run on each jet of the event, and the information is output to the ntuple for the highest energy jet in each hemisphere.

Patch VXEVNT: This patch contains a simple interface to the PYTHIA 6.1 event generator, including the routine `LCIBKV` which transfers the 4-vector information to the GEANT `KINE` and `VERT` banks, allowing the event to be simulated, including the preservation of all lifetime information.

To use this code, all the patches in `bvreco.car` and `vxuser.car` should be compiled with the standard BRAHMS code, excluding `bruser.car`. A suitable set of datacards (read by BRAHMS on the file `cardsfile`), is given below, typical of those used for the studies in this note.

```
C generate 100 events
trig 100
calopt 1
C don't attempt to read from event input file
kinfile 2
C turn on only tracking detectors TPC, ITC, FTD and VTX (CCD)
C      vtx itc ftd sit tpc bcal ecal coil yoke lumi mask bpipe pre quad hall
turnon  12   1   1   0   1   0    0    0    0    0    0    1     0   0    0
C centre of mass energy - by default PYTHIA generates e+e- -> f-fbar
ecms 91.2
C  set parameters for cone jet finder
jets 3 20 0.65 5.
end
```

Appendix B: Tagging performance parameterisations

For some physics studies outside of the BRAHMS framework, it may be useful to have parameterisations of the expected b and c-tagging performance. Therefore, the tagging efficiencies as a function of energy shown in Figure 12 have been parameterised, resulting in a standalone subroutine. This can be obtained from `richard.hawkings@cern.ch` or `/afs/desy.de/user/h/hawkings/public/bctpar.f`. The calling sequence is

[3] PYTHIA 6.1 is the first version of PYTHIA/JETSET where the event record `PYJETS` common block is in double precision. The `vxuser.car` code is designed for this, and it is thus difficult to make it work with JETSET 7.4, where the common block (here called `LUJETS`) is in single precision. Users are therefore recommended to use PYTHIA 6.1 wherever possible.

```
CALL BCTPAR(ITAG,EJET,TEFI,BEFI)
```

where `ITAG` gives the type of tag requested (1 for b-tag, 2 for c-tag), `EJET` the jet energy and `TEFI` the tagging efficiency for the tagged flavour. The subroutine returns the corresponding tagging efficiencies for the two 'background flavours' in the array `BEFI(2)`. Interpolation is used between the generated jet energy points of 45, 70, 100, 200 and 300 GeV. The parameterisation is not perfect, and in partucular underestimates the uds efficiency of the charm tag below charm efficiencies of about 30 %, but it should be useful for initial studies.

References

[1] Conceptual Design of a 500 GeV e^+e^- Linear Collider with Integrated X-ray Laser Facility, ed. R. Brinkman, G. Materlik, J. Rossbach and A. Wagner, DESY 1997-048, ECFA 1997-182.

[2] R. Hawkings and K. Mönig, Eur. Phys. J. Direct C8 (1999) 1.

[3] R. Brun et al., GEANT 3.21 users guide, CERN program library long writeup W5013.

[4] SIMDET version 3, A Parametric Monte Carlo for a TESLA Detector, M. Pohl, H.J. Schreiber, DESY 99-030.

[5] BRAHMS version 1.02, A Monte Carlo for a Detector at a 500/800 GeV Linear Collider, T. Behnke, G. Blair, M. Elsing, K. Mönig, M. Pohl, for a detailed description see `http:///www.hep.ph.rhbnc.ac.uk/ blair/detsim/brahms/summary.ps`.

[6] H.-U. Bengtsson and T. Sjöstrand, Comp. Phys. Comm. 46 (1987) 43;
T. Sjöstrand, Comp. Phys. Comm. 82 (1994) 74.

[7] OPAL collaboration, R. Akers et al., Z. Phys. C63 (1994) 197.

[8] OPAL collaboration, G. Abbiendi et al., Eur. Phys. J. C8 (1999) 217.

[9] ALEPH collaboration, D. Buskulic et al., Phys. Lett. B313 (1993) 535.

[10] D. Jackson, Nucl. Instrum. Methods A388 (1997) 247.

[11] SLD collaboration, K. Abe et al., Phys. Rev. Lett. 80 (1998) 660.

[12] DELPHI collaboration, P. Abreu et al., Eur. Phys. J. C10 (1999) 415.

[13] C. Peterson, T. Rögnvaldsson and L. Lönnblad, JETNET 3.0 - A Versatile Artificial Neural Network Package, LU TP 93-29, CERN-TH.7135/94.

[14] G. Bahan and R. Barlow, Identification of b jets using neural networks, MAN/HEP/92/1.

[15] R. Heuer, talk presented at the November 1999 meeting of the ECFA/DESY linear collider workshop, Obernai, France.

[16] C. Hensel, presented by T. Behnke at the November 1999 meeting of the ECFA/DESY linear collider workshop, Obernai, France.

[17] M. Elsing, The DELPHI silicon tracker in the global pattern recognition, DELPHI 99-147, linear collider note LC-TOOL-1999-008-TESLA.

[18] C. Damerell, transparencies presented at the July 1999 meeting of the ECFA/DESY linear collider workshop detector subgroup, CERN, Geneva, Switzerland.

[19] C. Hensel, private communication.

☺